

**Development of
chemical-hydraulic
models for the
prediction of the
long-term sealing
capacity of concrete
based sealing materials
in rock salt**

Development of chemical- hydraulic models for the prediction of the long-term sealing capacity of concrete based sealing materials in rock salt

Kyra Jantschik
Uwe Hertes
Thorsten Meyer
Helge C. Moog

August 2016

Remark:

This report was prepared under funding reference no. 02 E 11122 of the German Federal Ministry for Economic Affairs and Energy (BMWi).

The work was conducted by the Gesellschaft für Anlagen- und Reaktorsicherheit (GRS) gGmbH.

The authors are responsible for the content of this report.

Key Words:

Advection, Corrosion, Diffusion, Geochemical Modelling, Laboratory Tests, Permeability, Salt Concrete, Corel Concrete

Table of contents

1	Introduction.....	1
2	Einleitung	3
3	Description of the state of the art of experimental data of concrete based sealing materials	5
4	Characterisation of available concrete based sealing materials.....	10
4.1	Salt concrete.....	10
4.1.1	Mechanical properties.....	11
4.1.2	Hydraulic and chemical properties	12
4.1.3	Thermal Properties	14
4.2	Sorel concrete	14
4.2.1	Mechanical properties.....	15
4.2.2	Hydraulic and chemical properties	16
4.2.3	Thermal properties.....	16
5	Laboratory investigations	17
5.1	Batch-experiments.....	17
5.2	GRS Cascade Experiments	17
5.3	Diffusion experiments	20
5.4	Advection experiments.....	21
5.4.1	Experiments for investigating influence on porosity and permeability.....	22
5.4.2	Experiments for investigating reactions kinetics	24
6	Experimental results of short- and long-term investigations	26
6.1	Batch-experiments.....	26
6.1.1	Sorel concrete in contact with NaCl-solution	26
6.1.2	Sorel concrete in contact with Mg-rich-solution	30
6.1.3	Salt concrete in contact with NaCl-solution	32
6.1.4	Salt concrete in contact with Mg-rich-solution	35

6.1.5	Summary	38
6.2	Cascade experiments (preliminary results)	39
6.2.1	Cascade experiments with Sorel concrete and NaCl-solution	39
6.2.2	Cascade experiments with Salt concrete and Mg-rich-solution	42
6.3	Diffusion experiments	43
6.3.1	Through-diffusion experiments (pilot test)	43
6.4	Advection experiments.....	48
6.4.1	Sorel concrete in contact with NaCl- solution	48
6.4.2	Sorel concrete in contact with Mg-rich solution	51
6.4.3	Salt concrete – Gas permeability	53
6.4.4	Summary	54
6.4.5	Combined sample Sorel concrete/rock salt in contact with Mg-rich- solution	54
6.4.6	Combined sample Salt concrete/rock salt in contact with NaCl-solution...	56
6.4.7	Combined sample Salt concrete/rock salt in contact with NaCl- and Mg-rich solution	58
6.4.8	Summary	59
7	Description of the state of the art of related chemical process modelling.....	60
8	Predictive calculations of chemical processes	64
8.1	Geochemical modelling of Salt concrete in contact to IP21 solution.....	64
8.2	Geochemical modelling of MgO based concretes in contact to brines.....	66
8.2.1	Preliminary modelling results of cascade experiments in comparison to laboratory results	68
9	Conclusions	71
10	Zusammenfassung	74
	References	77

Tables	81
Figures	82

1 Introduction

The research leading to these results has received funding from the German Federal Ministry of Economic Affairs and Energy (BMWi) under contract no. 02E11122 and from the European Union's European Atomic Energy Community's (Euratom) Seventh Framework Programme FP7/2007-2011 under Grant agreement no 323273, the DOPAS project.

This report presents the current state of laboratory investigations and modelling activities related to the LAVA and LAVA-2 project. LAVA was performed by GRS as part of the European project DOPAS (Full scale Demonstration of Plugs and Seals) under WP 3 task 2 and WP 5 task 1 on “Design and technical construction feasibility of the plugs and seals” and “Performance assessment of plugs and seals systems”. In the LAVA project Sorel concrete was investigated. LAVA-2 is a national project in which same laboratory investigations and modelling activities are intended as in LAVA. But LAVA-2 deals with Salt concrete. This report presents results from LAVA and preliminary results from LAVA-2. Laboratory investigations and modelling activities will be completed in term of LAVA-2. At the end of the project, a GRS final summary report including relevant results from LAVA and LAVA-2 will be provided.

The work is related to the research and development on plugging and sealing for repositories in salt and is of fundamental importance for the salt option which represents one of the three European repository options beside clay and crystalline rock.

In the German concept for the final disposal of radioactive and hazardous wastes in salt formations Salt concrete and Sorel concrete are proposed as technical barriers (shaft and drift seals). Due to the specific boundary conditions in salt host rock formations these materials contain crushed salt instead of sand or gravel. The long history of sealing elements based on these materials is founded on the durability and persistency under environmental conditions. They have chemical and physical retention potential for nuclear waste and are tolerant against many solutions and materials.

However, depending on the solution composition, Salt concrete and Sorel concrete may be subject to some degree of degradation. Therefore, the safety assessment of the repository system implies detailed knowledge of their geochemical behaviour in the salt environment. In case of solution intrusion into the repository, the sealing elements made of Salt and Sorel concrete may be affected by significant changes regarding their

mineralogy, their chemical composition as well as their hydraulic and mechanical properties. The changes are due to dissolution and precipitation reactions, inducing changes in solution composition and pH value.

2 Einleitung

Die im Rahmen dieses Projektes durchgeführten Arbeiten wurden vom deutschen Bundesministerium für Wirtschaft und Energie (BMWi) unter der Fördernummer 02E11122 sowie von der Europäischen Atomgemeinschaft (Euratom) im siebten Rahmenprogramm FP7/2007-2011 unter Vereinbarung des DOPAS Projektes, 323273, gefördert.

In diesem Bericht wird der aktuelle Stand der Laboruntersuchungen und modelltheoretischen Arbeiten im Kontext der Projekte LAVA und LAVA-2 dargestellt. Das Projekt LAVA wurde von der GRS im Rahmen des europäischen Projekts DOPAS (Full scale Demonstration of Plugs and Seals) durchgeführt. Im Rahmen des EU-Projektes wurden verschiedene Versiegelungs- und Verschlusssysteme für geologische Tiefenlager getestet und weiterentwickelt. Das LAVA-Projekt ist den Vertikalprojekten 3, Aufgabenstellung 2 „Design und technische Konstruktionsmöglichkeiten für Verschluss- und Dichtelemente“ sowie Vertikalprojekt 5, Aufgabenstellung 1 „Bewertung der Ausführung von Dicht- und Verschlusselementen“ zugeordnet. LAVA-2 ist ein nationales Projekt, in welchem die gleichen Laboruntersuchungen und modelltheoretischen Arbeiten durchgeführt werden wie in LAVA. In LAVA wird der Baustoff Sorelbeton untersucht, in LAVA-2 hingegen Salzbeton. Im Rahmen dieses Berichtes werden die Ergebnisse der Untersuchungen am Sorelbeton dargestellt sowie die bislang vorliegenden Ergebnisse der Untersuchungen am Salzbeton. Mit Ende der Projektlaufzeit von LAVA-2 wird von der GRS ein Bericht zur Verfügung gestellt, der sowohl die Ergebnisse zum Sorelbeton als auch zum Salzbeton zusammenfasst.

In Europa existieren neben der Option Steinsalz noch die Möglichkeiten für eine Tiefenlagerung hochradioaktiver Abfälle in Ton- und Kristallin Gestein. Die Forschungsarbeiten zu den Verschlusskapazitäten verschiedener Dammbaustoffe im Steinsalz sind von fundamentaler Bedeutung für die Steinsalzooption.

Das deutsche Endlagerkonzept sieht für Endlager für hochradioaktive und toxische Abfälle vor, dass Strecken und Zugangsschächte mit Dicht- bzw. Verschlusselementen aus Salz- bzw. Sorelbeton verschlossen werden sollen. Aufgrund der speziellen Randbedingungen im Steinsalz beinhalten Salz- und Sorelbeton Salzgrus als Zuschlagsstoff anstelle von Sand oder Kies. Diese Spezialbetone zeichnen sich durch eine hohe Dauerhaftigkeit und Beständigkeit aus, sind beständig gegenüber vielen verschiedenen Lö-

sungen und Materialien und haben das Potential nukleare Abfälle sowohl physikalisch als auch chemisch zurückzuhalten.

Abhängig von der anstehenden Lösungszusammensetzung kann es jedoch auch am Salz- und Sorelbeton zu Schädigungen kommen. Dadurch werden unter anderem die chemische Zusammensetzung sowie die hydraulischen und mechanischen Eigenschaften des Betons beeinflusst. Es können Auflösungs- und Ausfällungsreaktionen auftreten, die Zusammensetzung der anstehenden Lösung kann sich verändern sowie der pH-Wert von Beton und Lösung. Dadurch kann es zu einer Beeinträchtigung des Abdichtungsvermögens eines solchen Dammbauelementes kommen, sodass es wichtig ist, die potentiellen (geochemischen) Prozesse an einem Verschlusselement in Kontakt zu salinaren Lösungen zu kennen.

3 Description of the state of the art of experimental data of concrete based sealing materials

Barrier materials are primarily intended to minimize solvent flow towards a location where hazardous substances are disposed of. As a secondary effect, such materials can also act as sorptive sink for solute contaminants, thereby further minimizing any harmful effects of contaminants on the biosphere.

Barrier materials commonly investigated are frequently referred to as “cement” or “cement based”. This denotation tends to obscure the fact, that these materials are chemically very different. Within the context of sealing boreholes or drifts in salt rock formations the following – rough – classification is appropriate:

- “Salt concrete”: usually a mixture of blast furnace cement and crushed salt (dominated by NaCl), made up with saturated NaCl-solution, most stable with aqueous solution whose composition is dominated by NaCl;
- “Sorel concrete”: usually a mixture of MgO and crushed salt (dominated by Halite), made up with 5 molal MgCl₂-solution, most stable with aqueous solutions whose composition is dominated by MgCl₂.

Corrosion processes in these materials are divided phenomenologically into leaching and swelling mechanisms. In leaching processes single solid phases will be dissolved leading to an increase of porosity and permeability. Swelling occurs if phases precipitate that have a higher volume than the starting phase assemblage. An overview of the corrosion processes is given in /BIC 68/, /HEW 98/, /SKA 02/.

In case of a salt environment highly saline solutions can be expected. In contact to these solutions (NaCl-rich and/or Mg-rich) degradation processes by combined magnesium and sulphate attack have to be taken into account. Therefore solutions with high Mg-, SO₄- and Cl-contents are considered to be most aggressive for Ca-based cements /BON 92/, /HAS 03/. Conversely, solutions with a high NaCl-content are considered to be most aggressive for Mg-based cements (“Sorel concrete”). Thus, for the present project, the primary issue is the reactivity of Sorel concrete with NaCl-dominated solutions and Salt concrete with Mg-rich solutions.

The chemical corrosion of Salt concrete is due to several processes:

- Mg corrosion – Dissolution of the network of CSH (Calcium silicate hydrate) phases and formation of MSH (Magnesium silicate hydrate) gels. The CSH phases react with Mg and sulphate from the solution and precipitate Gypsum, Brucite and silica gel. In the second step Brucite and silica gel form MSH phases and water.
- Gypsum corrosion - Dissolution of Ca(OH)_2 and CSH phases in the concrete matrix and precipitation of Gypsum ($\text{CaSO}_4 \cdot 2\text{H}_2\text{O}$).
- Cl corrosion – The mineral Friedel's salt ($3 \text{CaO} \cdot \text{Al}_2\text{O}_3 \cdot \text{CaCl}_2 \cdot 10 \text{H}_2\text{O}$) is formed if Cl-rich solutions react with calcium aluminate phases.

Chlorides are bound in cement based materials mainly through the formation of Friedel's Salt ($\text{C}_3\text{A} \cdot \text{CaCl}_2 \cdot 10\text{H}_2\text{O}$) and also to a limited extent in hydrate phases with iron instead of aluminum. Friedel's salt precipitates in response to chloride in the pore solution, i.e. changing chloride concentrations in the pore fluid also lead to different amounts of Friedel's salt /GRA 96/. The formation of Friedel's salt is associated with an increase in volume of the solid phase, which can lead to the destruction of the pore structure of the construction material ("impulsive attack"). For concrete itself the supply of chlorides is relatively innocuous, as long as not due to evaporation crystallization processes with corresponding pressures occur. In Salt concrete already appropriate amounts of Friedel's salt have been precipitated during the hardening process of the uncorroded material so that at a later access of chloride containing solution, no harmful volume increase by the formation of Friedel's salt takes place. Friedel's salt is one of the most stable chlorine containing phases in concretes. In Fig. 3.1 hexagonal plates of Friedel's salt are depicted. Additionally, CSH phases are covered with NaCl which slightly decrease the corrosion process due to aggressive agents.

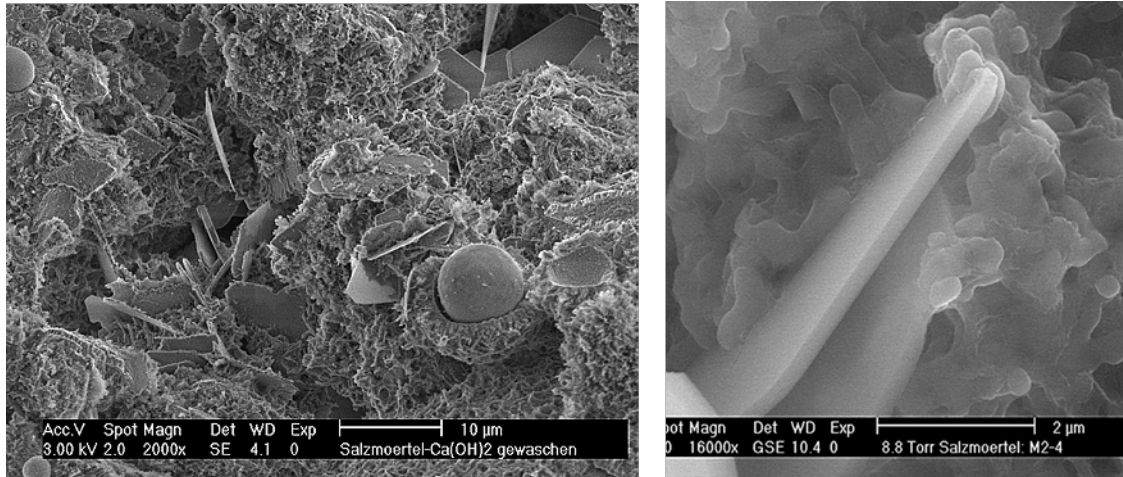
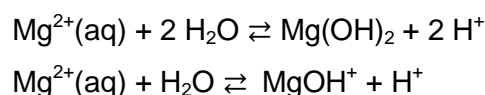


Fig. 3.1 CSH-phases in Salt concrete covered by Halite; Friedel's salt (hexagonal plates) /MEY 03a/

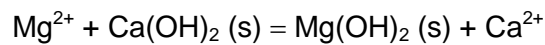
The chemical attack of sulphate on cement based materials depends on the attacking sulphate solution and the cement itself. The attack will result in an expansive reaction, a softening of the material, or a combination of these two reactions. Gypsum has a 17.7 % times higher molar volume than Ca(OH)_2 and destroys therefore the concrete. At high pH penetrating sulphate ions can form Ettringite, which occurs in the form of needle-like crystals /HEW 98/. The formation of Ettringite leads to the formation of cracks in the concrete. Prerequisite is a prior weakening of the concrete matrix by destruction of the CSH structure /MEH 00/. In the presence of high concentrations of chlorides or carbonates no Ettringite formation is found. The same was observed for high concentrations of magnesium in solution ($> 0.062 \text{ mol/l}$), due to the pH decrease to values of about pH 8-9 by Brucite formation; below pH 11.6 to 10.6 Ettringite decomposes into Gypsum /MEH 00/.

Magnesium has a potential to corrode cement based materials because magnesium salts are weaker dissociated in aqueous solution than calcium salts. Dissolved magnesium has a higher tendency to hydrolysis than calcium. Therefore magnesium-containing solutions have a slightly acidic character:



The pore water of fresh Portland cement has a high pH of about 13 caused by a dissolution of Portlandite Ca(OH)_2 . During the attack of magnesium-containing solutions on

Salt concrete, the structure-forming calcium hydroxide is first (if any) dissolved, while magnesium precipitates as Brucite (magnesium hydroxide).



When Portlandite is consumed in the cement body and no longer available as a buffer, the pH decreases to below pH 9 in the cement. At this pH, the CSH phases are no longer stable and decompose into silica and dissolved calcium /MEH 00/. This also applies to the CSH phases in blast furnace cements. Although there is no free Portlandite existing and the pH of the pore water is much lower, the attack of magnesium leads in the same way to the dissolution of CSH phases.

The precipitation of Brucite due to the alkaline conditions in the concrete pores is responsible for the partial clogging of these pores resulting in a slowing down of the corrosion process. In a later stage of the corrosion progress magnesium silicate hydrates (MSH) i.e. serpentine, talc or Kerolite precipitate. In contrast to CSH phases, the MSH phases develop no strength which will result in a softening of the material. Sulphate also present in solution reacts with the released calcium to Gypsum or Anhydrite. In summary, the strength-forming CSH phases in the cement are destroyed by the calcium to magnesium "replacement".

About the rate of the formation of magnesium silicates from magnesium hydroxide and free silica or calcium silicates only very limited data are available. /TEM 98/ observed the formation of magnesium silicate from magnesium hydroxide and silica by grinding a corresponding mixture of solids. The reaction seems to proceed through a partially existing solution phase, which results from the partial dehydration of the silica. The reaction is also observed during heating of a mixture of magnesium hydroxide, silica and water at 80 °C. Already after 24 hours under these conditions, the complete conversion of the silica into magnesium sheet silicates could be observed. The type of reaction products formed depends on the particular mixing ratios. /YAN 60/ observed products of talc and chrysotile at temperatures between 100 °C and 300 °C. However, these reactions could only be observed at high temperatures, their formation is unlikely under the expected conditions at a disposal site.

In aqueous medium and at moderate temperatures /BRE 05/ investigated the reaction of magnesium nitrate with sodium metasilicate. They observed MSH phases with a

Mg/Si ratio from 0.82 to 0.94 after an aging process of 6 months at 85 °C. The Mg/Si ratio of the formed MSH phases was therefore rather on the side of talc (3/4) than of chrysotile (3/2).

4 Characterisation of available concrete based sealing materials

4.1 Salt concrete

Salt concrete is a concrete which consists of a matrix from cement with inclusion of crushed salt. There are various mixtures of Salt concrete. The composition of Salt concrete used in LAVA-2 project consists of /ENG 08/, /MÜL 10/

- Blast furnace cement HOZ 25 HS/NW
- Crushed salt (grain size 0 to 16 mm) and
- NaCl-solution.

The proportion is defined in Tab. 4.1.

Tab. 4.1 Composition of Salt concrete /MÜL 10/ (Source gives total mass of components to 100 % but by addition it is only 99.9 %. Probably this deviation is not significant in context to the uncertainty of measurements.)

Component of Salt concrete	Proportion in [kg/m ³]	Proportion in mass-%
Blast furnace cement	380	18.3
Crushed salt	1496	72.1
NaCl-solution	198	9.5
Total	2074	100.0 (99.9)

Fig. 3.1 shows a Salt concrete sample. Crushed salt inclusions are clearly to identify by the dark points. Light grey area is the cement matrix.



Fig. 4.1 Salt concrete sample

For the present investigations Salt concrete samples derived from an in situ sealing element of a former German salt mine at the 945 m level. These samples were exposed to ambient conditions of a salt mine over ten years.

4.1.1 Mechanical properties

Mechanical parameters for Salt concrete were determined at samples from the in situ sealing element.

The bulk density of this type of Salt concrete is 2.074 kg/m^3 .

E-Modulus, Poisson ratio and uniaxial compression strength was determined at twelve specimens by uniaxial compression test /MÜL 10/. Uniaxial tensile strength was detected at only one specimen. The average values are summarized in Tab. 4.2.

Tab. 4.2 Mechanical parameters of used Salt concrete /MÜL 10/

E-Modulus [GPa]	Poisson ratio [-]	Uniaxial compression strength [MPa]	Uniaxial tensile strength [MPa]
14.7	0.13	38.28	1.94

Mechanical properties of Salt concrete are influenced additionally by contraction of the Salt concrete. Contraction occurs because of water loss or because of chemical transformations in the cement matrix referred to as autogenic contraction. The process of

contraction can result in generation of shrinkage cracks. In /MÜL 12a/ deformations as consequence of contraction are expected in a range of 0.1 to 0.5 mm/m. Investigations of Salt concrete after /ENG 08/ yielded, that no shrinkage cracks develop as a result of contraction in the cement matrix.

Furthermore it can be expected, that Salt concrete has a creep behaviour because of the high proportion of crushed salt and in response to the convergence of excavation in rock salt. Investigations to the creep behaviour of used Salt concrete were executed by GRS. Results are presented in project LASA.

4.1.2 Hydraulic and chemical properties

In the following section hydraulic and chemical properties are considered combined because of the close correlation of hydraulic and chemical processes.

Two different types of porosity were determined: On the one hand there is the effective porosity. This porosity describes the pores, which are available for percolation of solutions. On the other hand the solution-filled porosity was determined. Solution-filled porosity is around 12 %, the effective porosity is between 2 and 10 % /MÜL 10/. Values were determined to only two samples of Salt concrete. Here comparative values are needed.

The gas permeability was detected under a radial pressure of 1 MPa and a gas injection pressure of 0.6 MPa in GRS laboratory. In 80 % of the samples no permeability was measurable. In the remaining samples gas permeability was around $5 \cdot 10^{-20} \text{ m}^2$. Consequently Salt concrete samples are tight against solution.

Corrosion is a further process, which influences the hydraulic properties of Salt concrete. Corrosion can be generated by the influence of IP21 or NaCl-solution. If these solutions approach the sealing in a repository corrosion can occur by solving or degradation attack. Phases are removed from the construction material by solving attack. Afterwards porosity can increase and load capacity can decrease. Construction material experiences a volume increase by degradation attack because of regeneration of phases with higher volumes. This can result in damage of the construction material, if the volume increase cannot be contained in the pores of the Salt concrete /MEY 03/.

Corrosion depends on the composition of the reacting solution. Under repository conditions solutions may contain sulphates, magnesium and chlorides. The solutions are low acid and can generate different processes of corrosion.

Attack of sulphate can generate a softening or swelling of Salt concrete. Ettringite is comprised of sulphate, and magnesian-, aluminous- and ferruginous phases of the Salt concrete. The material softens if the mass of Portlandite of the cement matrix is consumed. Portlandite is consumed, because of the requirement of calcium for the formation of Ettringite. Normally Ettringite phase is more stable against Gypsum. If aluminum and iron are consumed or the components cannot be solved fast of the Salt concrete, generation of Gypsum insert. Also generation of Gypsum insert, if pH values is too small, because in that case, Gypsum is more stable against Ettringite.

Presence of magnesium can also result in a softening of Salt concrete. First calcium hydroxide in the cement matrix dissolves. Afterwards, components of calcium of the calcium-silicate-hydrate-phases (CSH-phases) are dissolved until they are completely consumed. The pore solution of Salt concrete is alkaline, so resolution of magnesium hydroxide is preferred. Magnesium hydroxide plugs the pores of Salt concrete and decelerates corrosion by magnesium for a certain time span. Finally magnesium-silicate-hydrates are formed. They have a small stability and completely destroy the matrix.

Additional the pH influences the stability of Salt concrete. Salt concrete is thermodynamically instable in neutral and acid milieus. The present solutions have a pH of 6. Calcium hydroxide is dissolved in low pH. Alkaline buffer capacity of pore solution is lost as the result of consumption of calcium hydroxide. Other cement phases become instable, too and dissolve. If all CSH-phases are dissolved, the construction material is destroyed. However, this process is not the main cause for corrosion of Salt concrete because corrosion processes described before are more significant /MEY 03/.

Summarized descriptions before declare, that Salt concrete is stable against NaCl-solutions and is corroded by magnesian- and sulphate-containing solutions including IP21-solutions. This statement is constrained by /KRA 08/.

4.1.3 Thermal Properties

Thermal properties of Salt concrete are defined by specific heat, thermal conductivity and thermal expansion coefficient. The parameters, which were detected for used Salt concrete are summarized in Tab. 4.3.

Tab. 4.3 Thermal properties of used Salt concrete /MÜL 12b/

Specific heat c_p [J/(kg*K)]	Thermal conductivity λ [W/(m*K)]	Thermal expansion coefficient α [1/K]
1.0	1.14	$4.0 \cdot 10^{-5}$

The focus of further works is the investigation of the chemical and hydraulic behaviour of Salt concrete. Hence thermal properties are not specified.

4.2 Sorel concrete

Preferred mixture is Sorel concrete A1 /FRE 15/, which consists of

- Magnesium oxide (Reactivation: 200-250 s after citric acid test)
- Crushed salt (grain size max. 4 mm)
- $MgCl_2$ -solution (5 molal).

Reactivation of Magnesium oxide and molality of $MgCl_2$ -solution are given by /FRE 15/. The mass ratio is given by /TEI 09/ (Tab. 4.4).

Tab. 4.4 Composition of Sorel concrete A1 /TEI 09/

Component of Sorel concrete	Proportion in [kg/m ³]	Proportion in mass-%
Magnesium oxide	218	11.3
Crushed salt	1237	63.7
$MgCl_2$ -solution	485	25.0
Total	1940	100.0

Fig. 4.2 shows a Sorel concrete sample with crushed salt (darker areas) and magnesium oxide matrix (light areas).



Fig. 4.2 Sorel concrete sample

Sorel concrete A1 is a 3-1-8 mixture, which means that during hydration $3\text{MgOH}\cdot\text{H}_2\text{O}\cdot 8\text{MgCl}_2$ is preferentially formed (so called 3-1-8-phase). Therefore it is necessary to use magnesium oxide and MgCl_2 -solution as described before /FRE 15/. 3-1-8 phases are characteristic for Sorel concrete. Sorel concrete samples were produced at GRS laboratory.

4.2.1 Mechanical properties

Values for mechanical properties are based on investigations of DBE on Sorel concrete A1. Investigations of mechanical properties of GRS produced samples were not yet completed. Density is around 1.940 kg/m^3 .

Tab. 4.5 Mechanical properties of Sorel concrete A1 /TEI 09/

E-Modulus [GPa]	Poisson ratio [-]	Uniaxial compression strength [MPa]	Uniaxial tensile strength [MPa]
21.8	0.24	36.5	2.37

4.2.2 Hydraulic and chemical properties

Porosity of Sorel concrete was determined in tests by DBE. It was determined for non-compacted and compacted samples. Average porosity for non-compacted samples is around 19.7 V%, for compacted samples around 17.9 V% /TEI 09/.

In GRS laboratory gas permeability of Sorel concrete A1 was determined on 22 samples under a surrounding pressure of 1 MPa and an injection pressure of 0.6 MPa. Average permeability is around $2.24 \cdot 10^{-18} \text{ m}^2$. This corresponds to an average gas permeability of $4.5 \cdot 10^{-18} \text{ m}^2$, which was determined at an in-situ sealing element of Sorel concrete A1 /TEI 09/.

With regard to Salt concrete corrosion NaCl- und Mg-rich-solutions have to be considered. Former investigations have shown that Sorel concrete corrodes in the presence of NaCl-solution, featured by the dissipation of the characteristic 3-1-8-phase. Dissolution of Sorel concrete stops if NaCl-solution has reached an adequate Mg-concentration /KUD 13/. The Porosity increases by the dissolution of 3-1-8-phases. This results in an increase of permeability. In the presence of solutions containing MgCl_2 0.5 mol/kg H_2O or higher, no corrosion of Sorel concrete is expected /KRA 08/.

4.2.3 Thermal properties

Thermal properties of Sorel concrete are also defined by specific heat, thermal conductivity and thermal expansion coefficient. The parameters, which were detected for used Sorel concrete A1 are summarized in Tab. 4.6.

Tab. 4.6 Thermal properties of Sorel concrete A1 (for samples dried at 60°C) /TEI 09/

Specific heat c_p [J/(kg*K)]	Thermal conductivity λ [W/(m*K)]	Thermal expansion coefficient α [1/K]
1295	2.22	$34 \cdot 10^{-6}$

5 Laboratory investigations

In long term safety analyses the evolution of permeability of sealing structures over time are key elements. Permeability controls the amount of solution which can access the waste and mobilise and transport radionuclides. The permeability of the initial uncorroded material is well known. The material design results in a low permeability of $k < 10^{-18} \text{ m}^2$. This important boundary condition ideally should not change over time. To account for chemical interactions between solution and sealing material batch- and cascade leaching experiments were performed, accompanied by analyses of reacted solution and solid phase composition. Furthermore, transport experiments (diffusion and advection) will be used to determine the velocity of the corrosion and the porosity/permeability changes of the Salt concrete as a function of solution composition and solution pressure.

5.1 Batch-experiments

Batch-experiments are simply tests for estimation of equilibration time between a powdered concrete and a saline solution. Powdered concrete and saline solution was brought in contact in PE-bottles in a defined solid-solution ratio. Bottles were agitated by hand once a day. After 2, 4, 7, 9, 11 and 18 days a solid and a fluid sample was taken during the main test. Further samples were taken after 46/88 and 158/200 days for a long term observation of solution and phase composition. An access of CO_2 to moist concrete is to be prevented because of carbonation. Composition of fluid samples was analysed by ICP-OES and ICP-MS and phase composition of solid samples was analysed by x-ray diffraction. On the basis of batch-experiments the duration of one cascade for GRS cascade experiment was determined (see chapter 5.2). Batch-experiments were executed in systems Sorel concrete/NaCl-solution, Sorel concrete/Mg-rich-solution, Salt concrete/NaCl-solution and Salt concrete/Mg-rich solution.

5.2 GRS Cascade Experiments

An experimental procedure, the so-called "cascade experiment", was developed for the investigation of the chemical reaction path of chemical hazardous wastes and concretes in contact to solutions /HER 96/, /HER 98/. Fig. 5.1 shows the scheme of this procedure which is based on a succession of batch-experiments (cascades). Basically

the cascade experiment is a titration experiment, each step or cascade is an own batch-experiment.

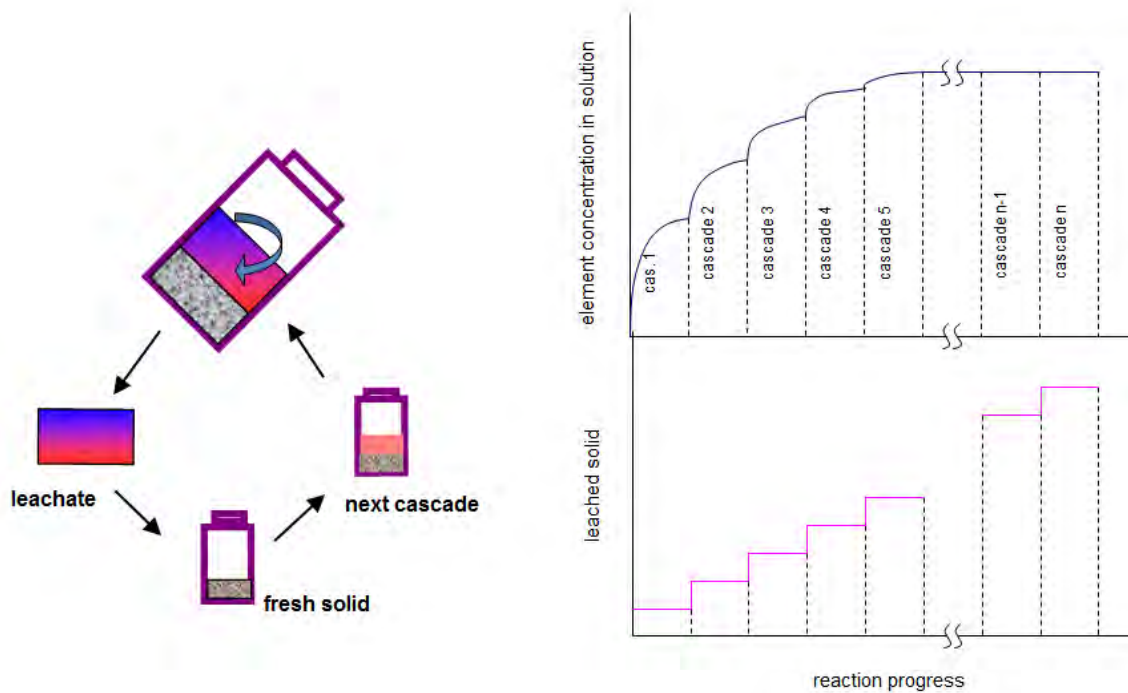


Fig. 5.1 Principle of cascade leaching experiments /HER 96/, /MEY 02/

In the first step a certain volume of fine grained solid is mixed with a certain volume of solution. The reaction takes place in an air tight vessel which is shaken continuously in an overhead rotator. After several days all soluble components of the solid are leached. The new solution composition is assumed to be in chemical equilibrium with the amount of added solid. Now the solution is separated from the solid and transferred to another vessel where new solid is added. This procedure is repeated for several times. During the succession of these batch-experiments in each step more solid is added to the initial solution volume. In each step the solid/solution ratio is kept constant. After each step only a part of the initial solution volume can be recovered and used in the next cascade. Therefore the number of cascades is limited by the steadily decreasing eluate.

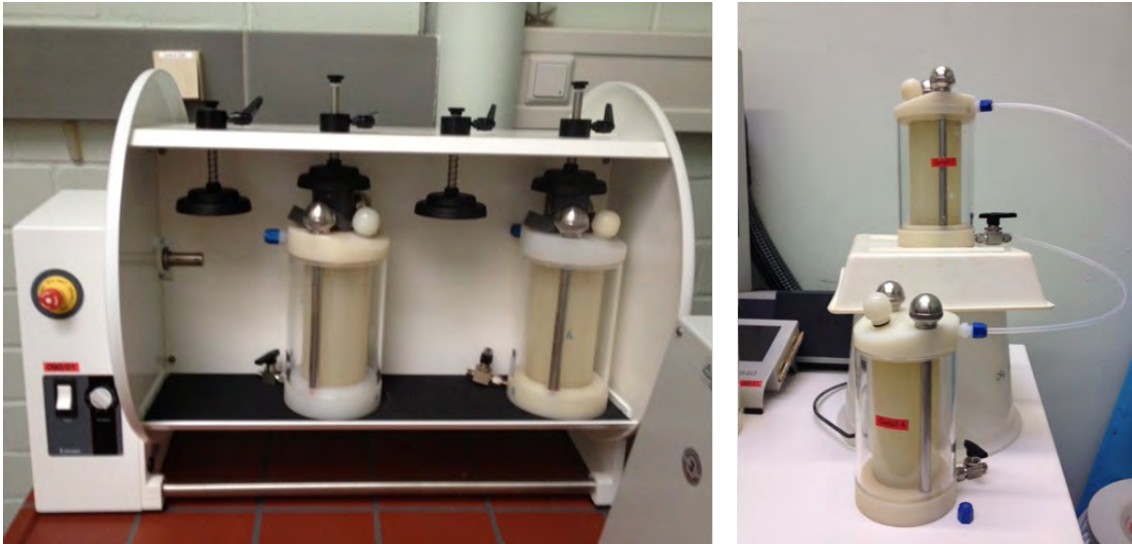


Fig. 5.2 Experimental set-up of the batch/cascade experiment

Main boundary conditions for cascade experiments are:

- grain size and mass of the solid
- solution composition and mass of the solution
- solid/solution ratio
- temperature
- vessel filled with argon
- stirring or rotation regime

The cascade experiment is conducted at $25\text{ °C} \pm 1\text{ °C}$ in plastic vessels to avoid the vessel corrosion (Fig. 5.2). Furthermore, the vessels had been flushed by argon gas. The experiment is carried out with a solid/solution ratio of 0.33. 100 g concrete and 300 g of solution are used in beginning of experiment. Mass of solutions reduces with each cascade. As a result the concrete mass has to be adapted to maintain the correct solid/solution ratio. Duration of one cascade is determined by batch-experiments before.

The total chemical reaction path of solution penetrating a geotechnical barrier can be reproduced by the cascade experiment until thermodynamic equilibrium between the original solution and the solid material is attained. In this way, chemical reactions which

may occur by an intrusion of solution to a sealing element can be simulated in very short time /NIE 14/.

5.3 Diffusion experiments

Diffusion experiments aim to investigate the diffusive transport process and its effect to concrete corrosion. Additionally diffusion coefficients can be determined. Two types of diffusion experiments are executed:

- In-diffusion experiment
- Through-diffusion experiment

Construction of in-diffusion experiments is very simple. Cylindrical concrete samples are coated in araldite with the exception of one end face, which is not sealed. Prepared samples were placed in a gas-tight box filled with NaCl- respectively Mg-rich-solution (CO₂-exclusion).

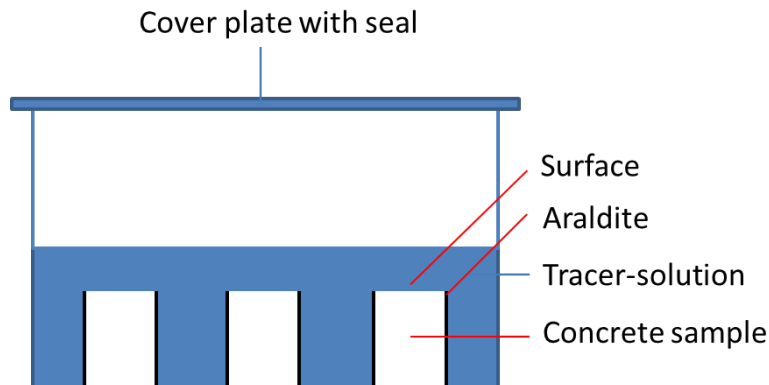


Fig. 5.3 Layout of in-diffusion experiments

Due to the concentration difference tracer from solution penetrates the samples. The diffusion coefficient can be determined by identification of the profile of intrusion. Therefore samples are to be analysed in layers.

Through-diffusion experiments complement in-diffusion experiments because diffusion coefficients in concrete are very low. It is assumed that through-diffusion experiments give results faster than in-diffusion experiments.

These experiments are executed in special diffusion cells. A simplified scheme is shown in Fig. 5.4. The concrete sample is installed in the diffusion cell and a tracer-spiked solution is passed on the bottom of the sample. A second, non-spiked solution is passed on the top of the sample and is analysed with regard to its tracer concentration over time. Because of the concentration difference between solution 1 (spiked) and solution 2 (non-spiked) a diffusional transport of tracer from the bottom to the top of the sample is expected.

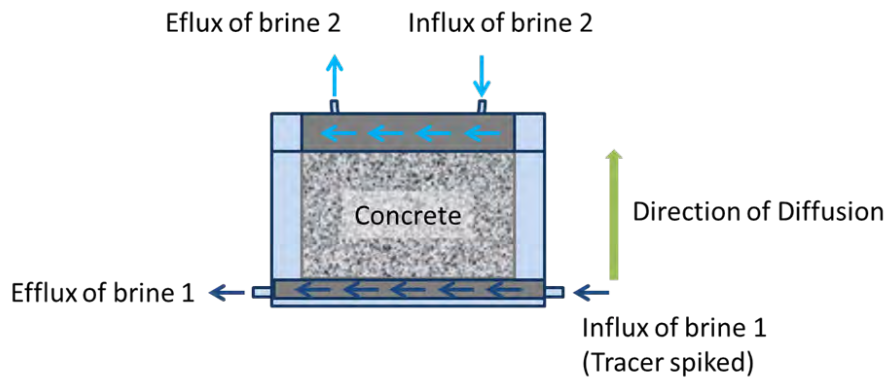


Fig. 5.4 Simplified construction of a diffusion cell

The diffusion coefficient can be calculated on the basis of these experimental data. The thickness of samples and the duration necessary for saturation prior to starting diffusion experiments is determined in preparatory experiments.

Through-diffusion-experiments aim furthermore at investigating the kinetics of chemical reactions by diffusive corrosion processes. In principle, two scenarios are conceivable: on one hand a parallel progression of diffusion and corrosion may occur, on the other hand diffusion may occur faster than the process of corrosion. This circumstance will be investigated by analyses of the solid sample using x-ray diffraction.

5.4 Advection experiments

Advective transport is another transport mechanism in porous media which may affect corrosion of sealing elements. Corrosion as a result of advective transport and its consequences for the long-term sealing capacity will be investigated in two types of advection experiments: experiments for investigating the influence of corrosion on porosity

and permeability of the sealing material and experiments which aim at reaction kinetics similar to diffusion experiments.

5.4.1 Experiments for investigating influence on porosity and permeability

These experiments are executed with two types of samples. The first type is a singular concrete sample which is loaded with fluid pressure (20 bar, NaCl-/Mg-rich-solution) on one end face. The effluent solution is collected on the other face. The sample surface is pressure-less cast in araldite in an advection cell. A simplified sketch of an advection cell is shown in Fig. 5.5. Samples are 10.0 cm in length and have a diameter of 5.0 cm.

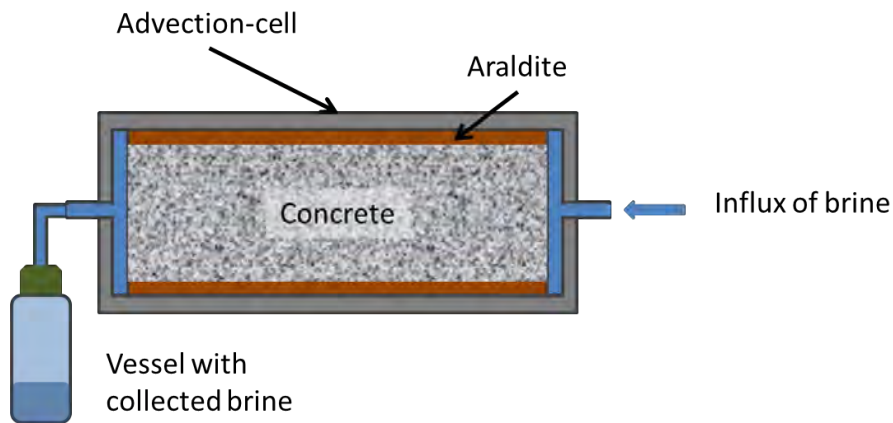


Fig. 5.5 Construction of an advection cell

In regular intervals vessels for collecting solution are substituted and permeability is calculated by Darcy's law on basis of mass of collected solution. The individual solution samples are analysed with regard to their composition. Additionally, the composition of each concrete sample is investigated by x-ray-diffraction. A conclusion and better understanding of corrosion mechanisms affected by advection processes in concrete is expected from these experiments.



Fig. 5.6 Experimental set up of advection experiment in laboratory

The second type of samples is a combined sample. The cylindrical concrete samples are surrounded by rock salt, thus exhibiting a circular contact zone. It is assumed that the contact zone is the primary pathway for solution and hence for the migration of radionuclides.

For these tests samples hollow rock salt cylinders with a Salt concrete respectively Sorrel concrete core are used. The concrete core is coated with salt slurry and afterwards inserted in the hollow salt cylinder (Fig. 5.7). Samples are exposed to a confining pressure until permeability is minimized. This process simulates salt creep on the sealing element. While the sample is compacted a non-corrosive saline solution passes the

sample: for samples with Salt concrete NaCl-solution is used and for samples with Sorrel concrete Mg-rich-solution. Afterwards, samples are placed in advection cells in the same manner as described before for pure concrete samples. Combined samples are 10.0 cm in length and have a total diameter of 7.0 cm. The diameter of the concrete core is 3.5 cm.

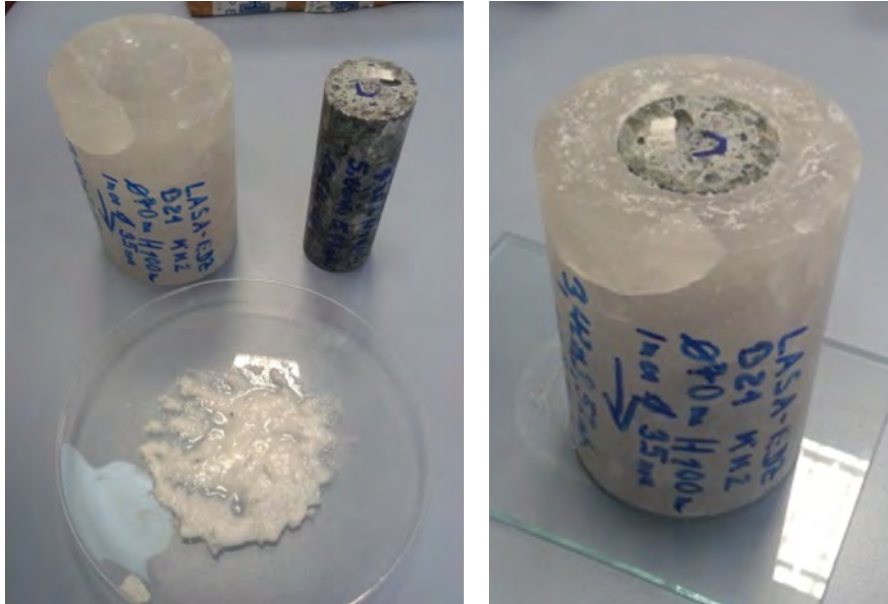


Fig. 5.7 Production of combined samples

5.4.2 Experiments for investigating reactions kinetics

The experimental set-up for investigating reaction kinetics in advection experiments is identical to advection experiments described before. The main difference is that samples are not passed through by solution continuously. Instead experiments are executed as “stop-and-flow”: in doing this solution remains stagnant in the pores of the samples for a defined time. Afterwards solution is collected in the same manner as described before and the new permeability is calculated. This execution of advection experiments offers the possibility to check if solution and concrete was balanced during flow-through of solution (phase 1 of advection experiments). If solution and concrete was not balanced because solution passed the concrete sample too fast, an increase of permeability is expected in “stop-and-flow” experiments.

Both phases of advection experiments could be executed at the same sample. Influence of solution to porosity and permeability was investigated in the first months of ad-

vection experiments. During this experimental phase solutions could penetrate the concrete samples the whole time. After no change in permeability was measurable anymore “stop-and-flow” experiments were conducted at the same samples.

6 Experimental results of short- and long-term investigations

6.1 Batch-experiments

Following chapter presents analysis of concrete and solution samples of batch-experiments. The diagrams of x-ray-diffraction show measured diffraction pattern of various concrete samples and are generally presented in red lines. Fig. 6.2 shows three diffraction patterns in parallel, coloured in red, blue and green. Significantly reflexes are labelled. Characteristic reflex lists of defined phases are shown additionally by vertical, various coloured lines below the diffraction pattern.

6.1.1 Sorel concrete in contact with NaCl-solution

Fig. 6.1 shows the x-ray-diffraction (XRD) diagram of Sorel concrete before contact with solution and Fig. 6.2 shows results after 18 days of contact with NaCl-solution.

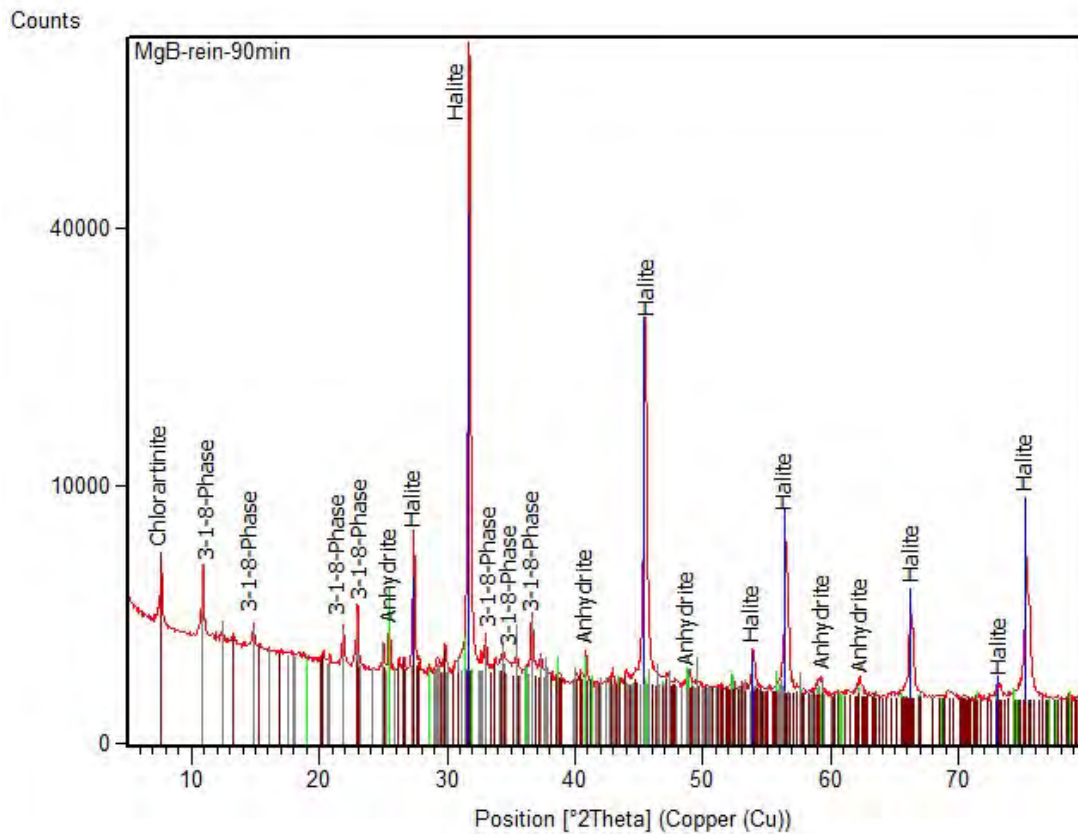


Fig. 6.1 Phase composition of Sorel concrete A1 before contact with solution

Sorel concrete A1 consists of characteristic sorel phases (3-1-8-phases), Anhydrite (CaSO_4) and Halite (NaCl). Chlorartinite ($\text{Mg}_2(\text{CO}_3)\text{Cl}(\text{OH})\cdot 3\text{H}_2\text{O}$) is a product of carbonation and results from earlier preparation of Sorel concrete, where CO_2 was not excluded.

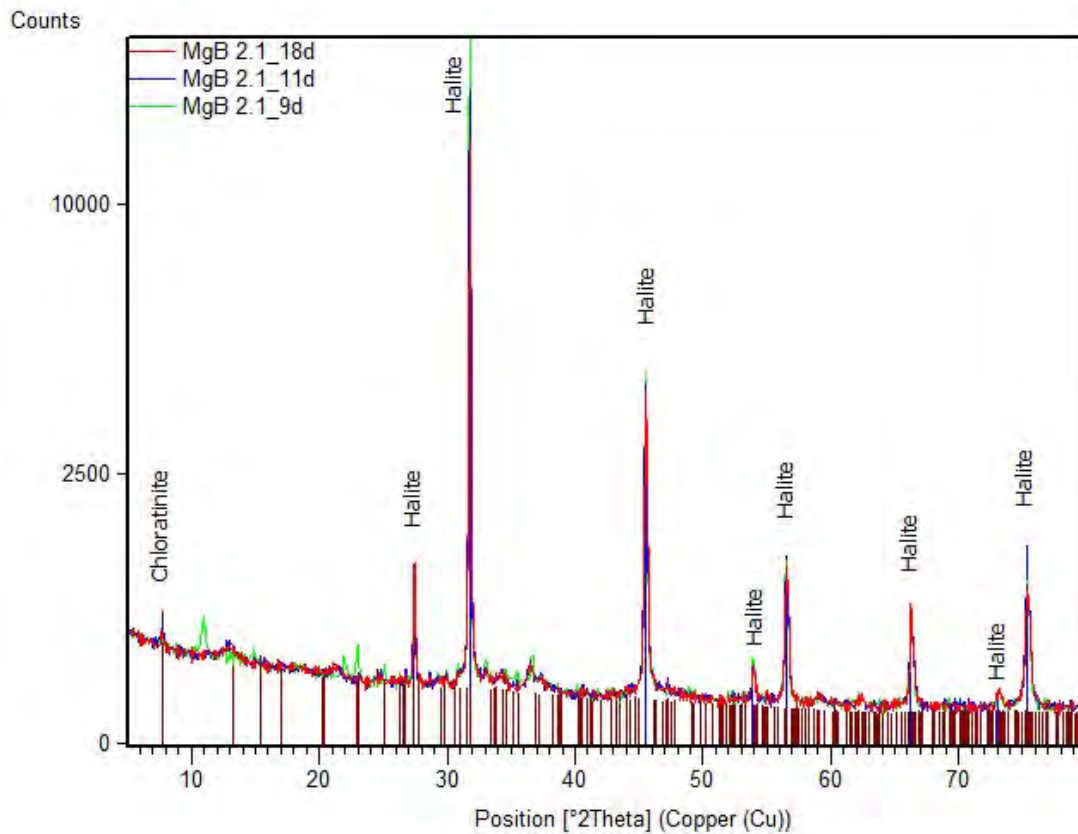


Fig. 6.2 Phase composition of Sorel concrete A1 after 9, 11 and 18 days of contact with NaCl-solution

After contact with NaCl-solution the dissolution of Sorel concrete typical 3-1-8-phases could be observed. Halite and Chlorartinite remain stable. Fig. 6.2 shows x-ray diffraction diagrams after 9 (green line), 11 (blue line) and 18 (red line) days reaction time. Phase composition changed up to 11 days. Afterwards no further significant change could be observed.

The analysis of the solution revealed no significant change in its composition over the main testing time of 18 days (see Fig. 6.3). But batch-experiments are still in progress. An analysis of solution after 90 days showed a small decrease of sulphate and magnesium and a clear decrease of sodium and chloride of circa 20 %.

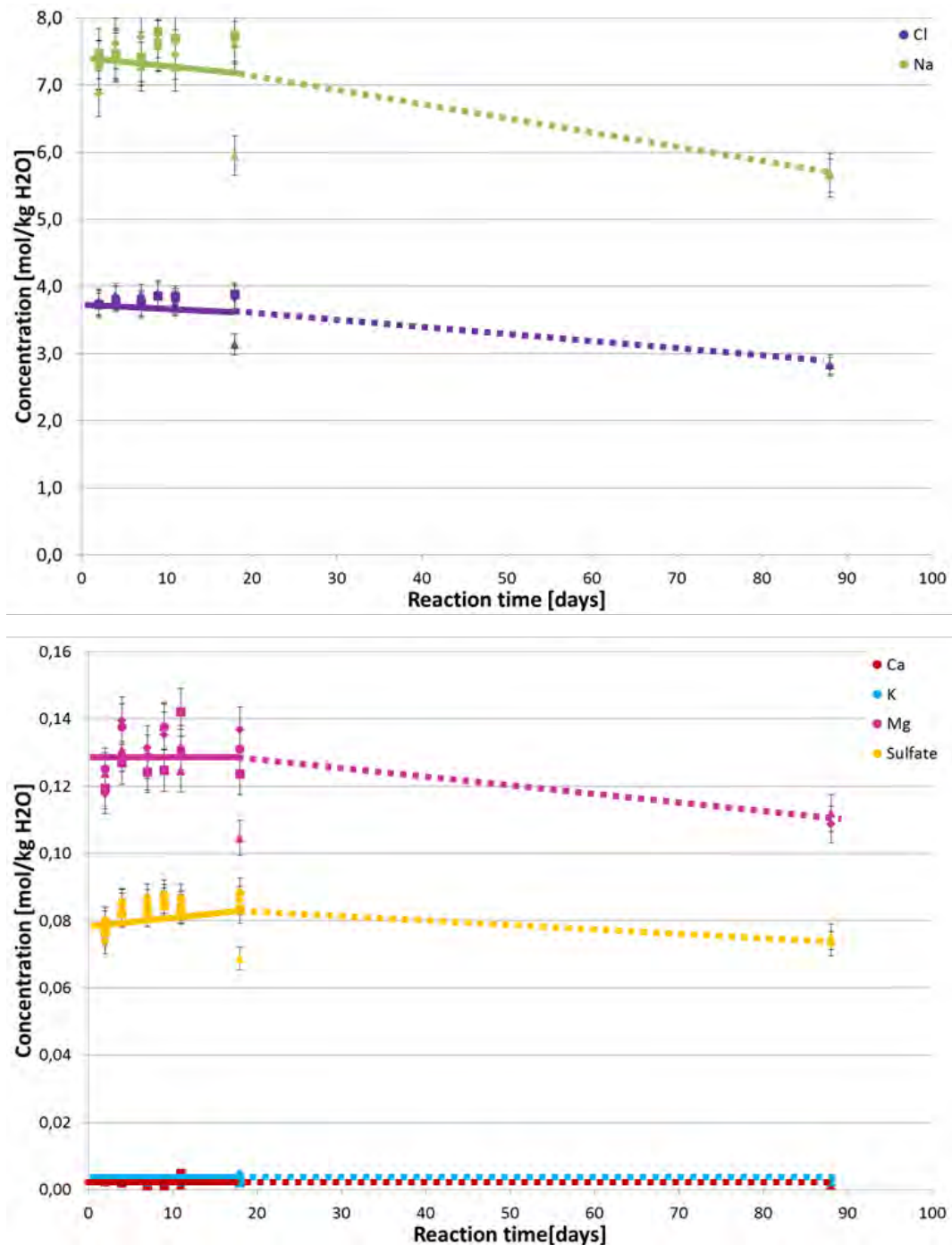


Fig. 6.3 Development of Cl, Na, Ca, K, Mg and sulphate concentrations in batch-experiments in the system Sorel concrete/NaCl-solution. Black bars describe errors of 5 %.

X-ray diffraction of solid samples after 90 days of contact with solution still needs to be done. Probably a change in phase composition can be observed correspondent to change of solution composition.

6.1.2 Sorel concrete in contact with Mg-rich-solution

Contrary to expectations the investigation of the system Sorel concrete/Mg-rich-solution showed a change in phase and solution composition. X-ray-diffraction showed a generation of Bischofite ($\text{MgCl}_2 \cdot 6\text{H}_2\text{O}$) and Carnallite ($\text{KMgCl}_3 \cdot 6\text{H}_2\text{O}$) (Fig. 6.4).

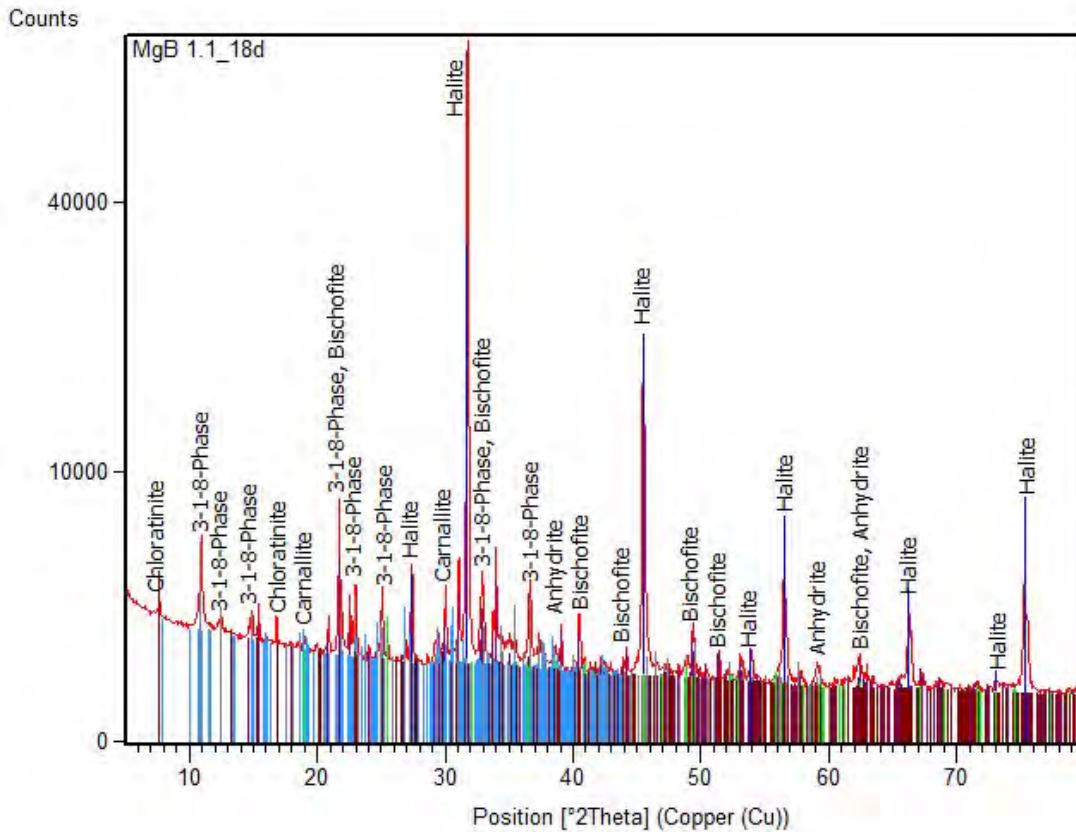


Fig. 6.4 Phase composition of Sorel concrete after contact to Mg-rich-solution

Solution analysis shows that concentrations of Na, Cl and Mg decreased during the test. Concentrations of K and sulphate decreased up to eleven days. Afterwards concentrations of K and sulphate increased slowly. Fig. 6.5 shows exemplarily the development of element concentrations in solution. The decrease of Mg, K and Cl concentrations corresponds to an increase of Bischofite and Carnallite in the solid phase.

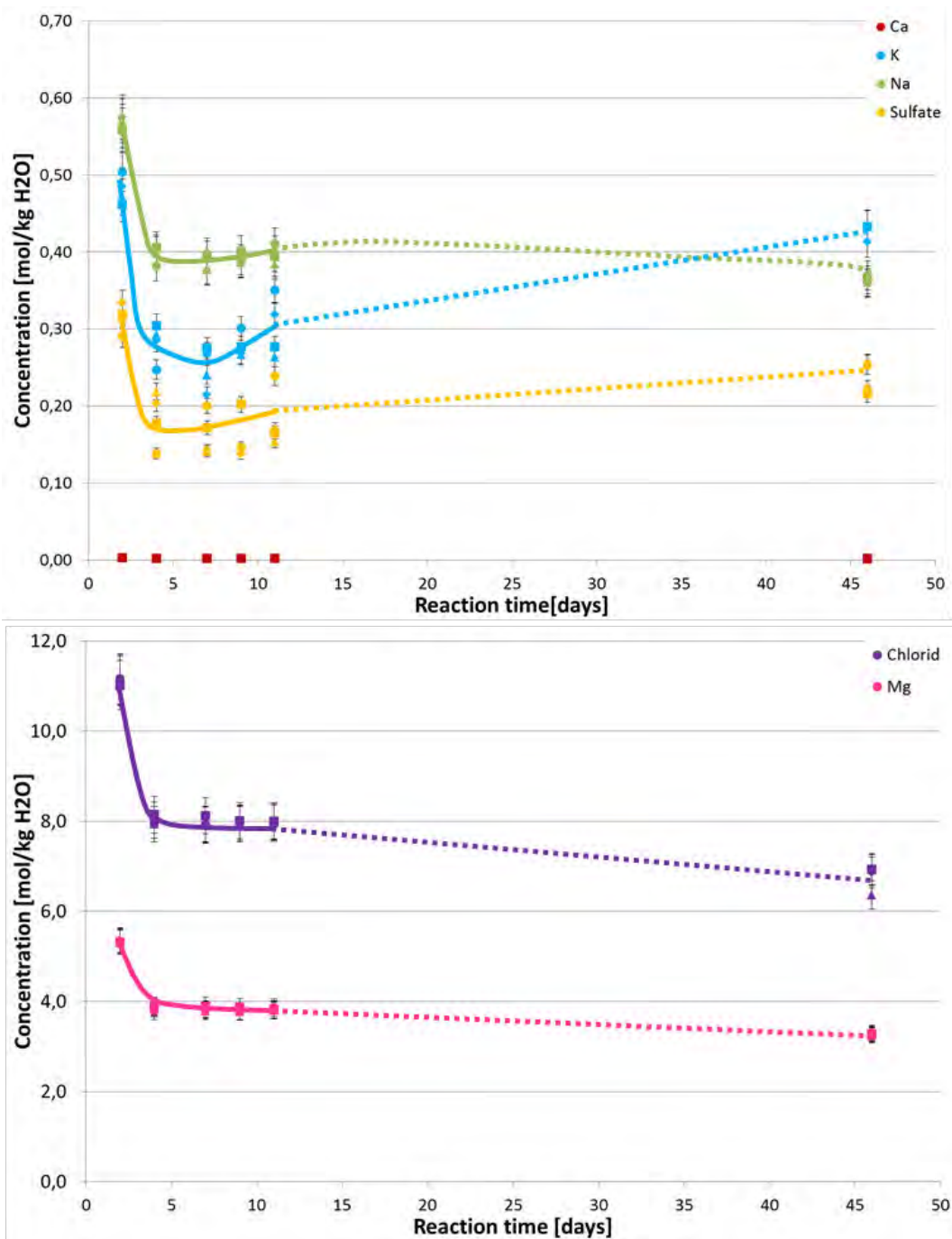


Fig. 6.5 Development of Ca, K, Na, Sulphate, Cl and Mg concentrations in batch-experiments in the system Sorel concrete/Mg-rich-solution. Black bars describe errors of 5 %.

X-ray diffraction of concretes after 45 days of contact with Mg-rich-solution still needs to be done. Probably dissolution of phases can be identified correspondent to an increase of the elements identified by solution analysis.

6.1.3 Salt concrete in contact with NaCl-solution

Fig. 6.6 shows the phase composition of Salt concrete before contact to any solution. It consists of Halite (NaCl), Anhydrite (CaSO_4), Friedels salt ($3\text{CaOAl}_2\text{O}_3\text{CaCl}_2 \cdot 10\text{H}_2\text{O}$), Portlandite ($\text{Ca}(\text{OH})_2$), and Coesite (SiO). Characteristic CSH-phases could not be identified by x-ray diffraction, probably because these phases are amorphous.

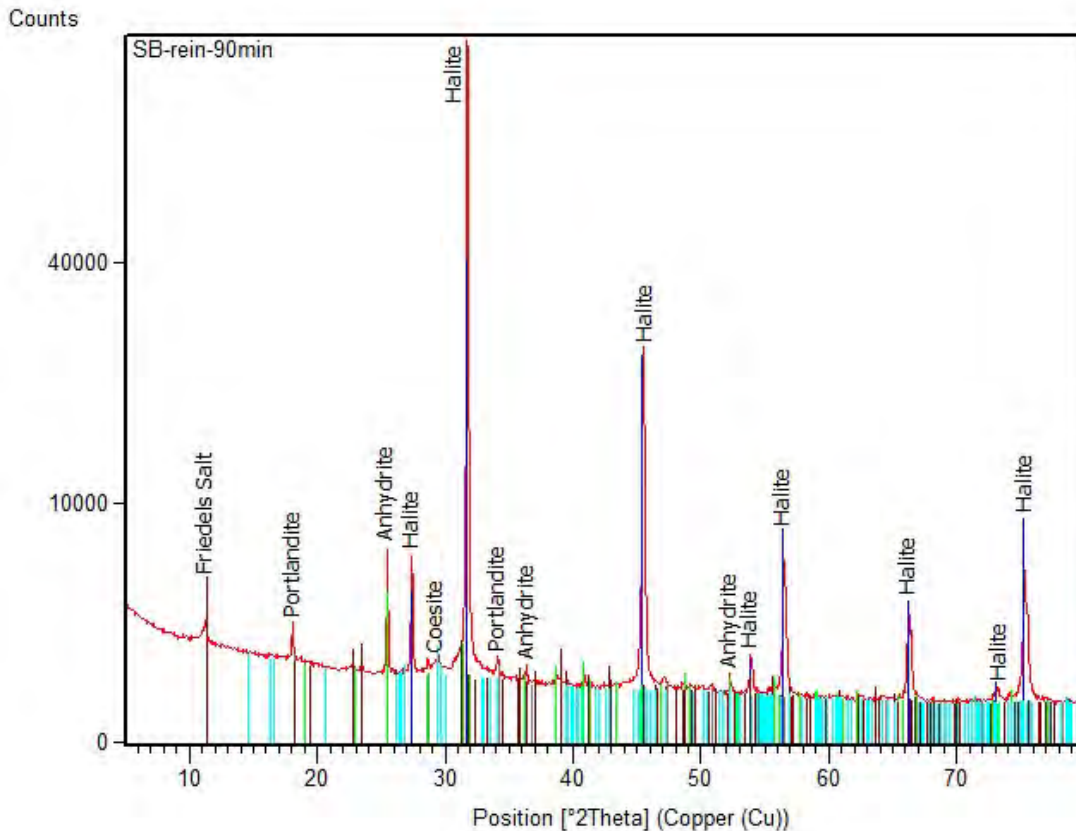


Fig. 6.6 Phase composition of Salt concrete before contact with solution

Salt concrete is produced with a saturated NaCl-solution hence its composition does not change significantly in contact with this solution. Fig. 6.7 shows the phase composition of Salt concrete after 18 days of contact with a saturated NaCl-solution. The x-ray diffraction shows only the dissolution of Portlandite.

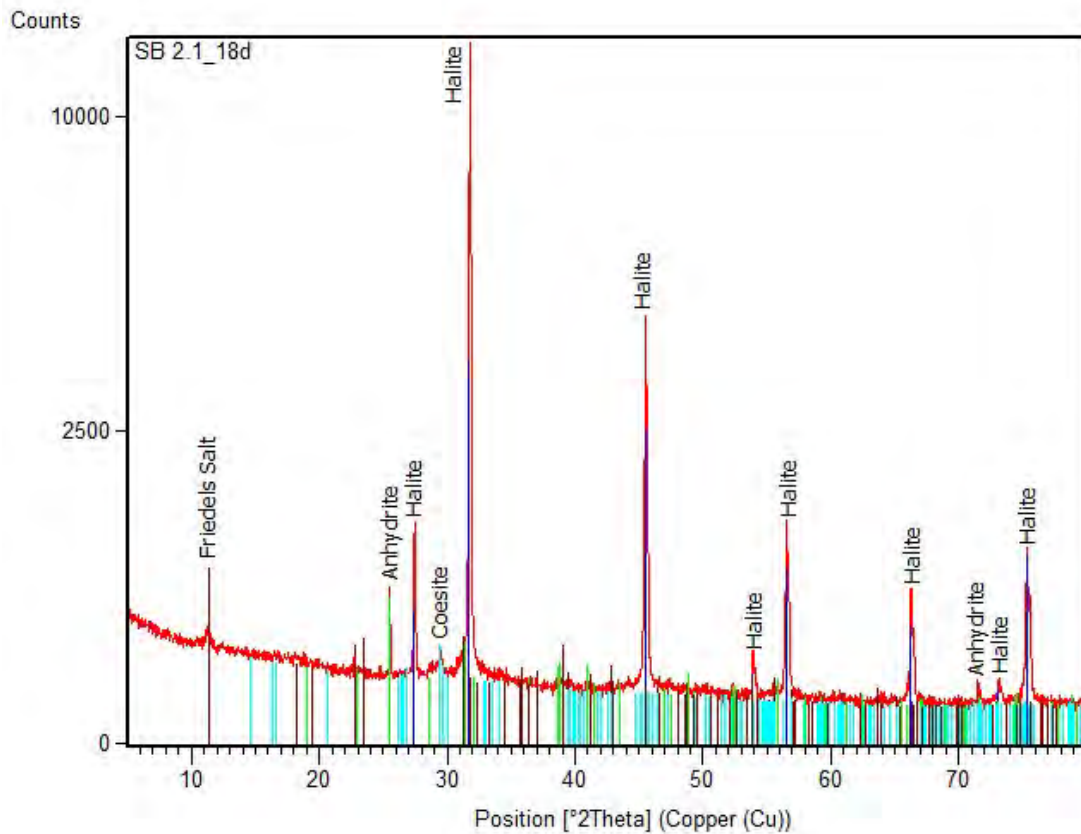


Fig. 6.7 Phase composition of Salt concrete after contact to NaCl-solution

Consideration of solution composition showed, that there was no significant change in solution during the first 18 days. The most significant change was the small increase of sulphate. This could result from the dissolution of Anhydrite, which is included in the crushed salt of Salt concrete. But if Salt concrete was in contact to saturated NaCl-solution over 90 days, concentrations of sulphate, Ca, K and Si decreased less. Na and Cl concentrations decreased clearly around 25 % (Fig. 6.8).

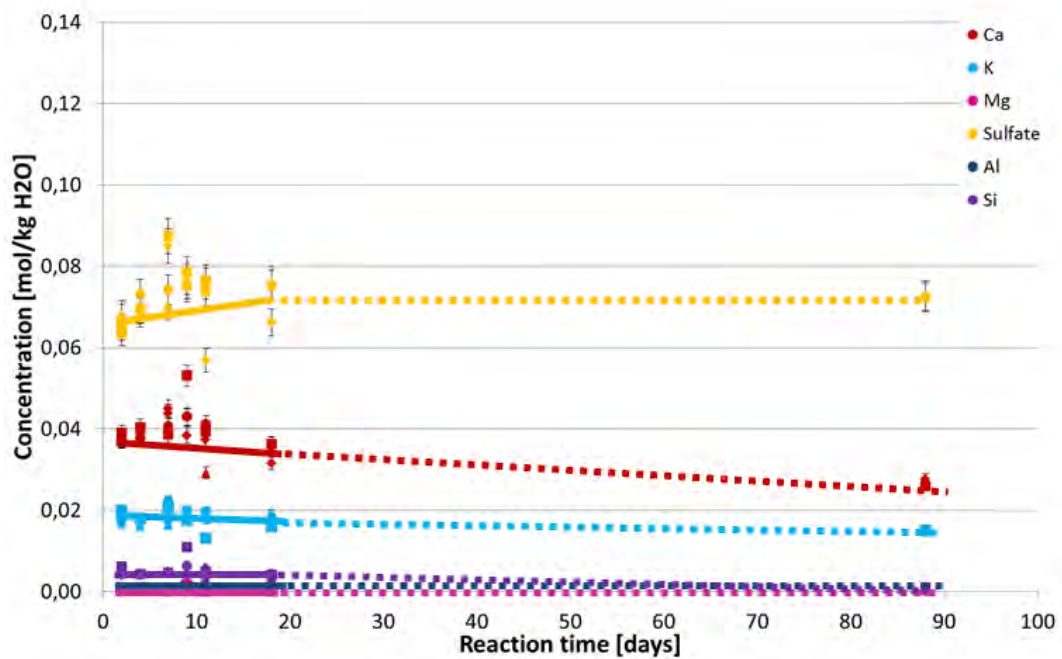
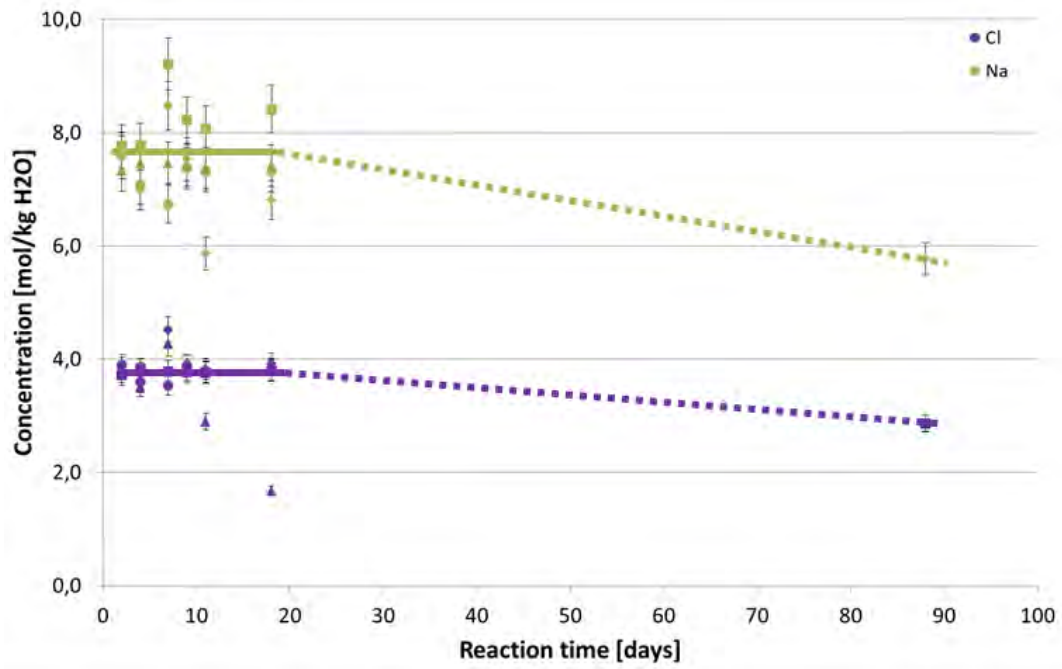


Fig. 6.8 Development of Cl, Na, Ca, K, Mg, sulphate, Al and Si concentrations in batch-experiments in the system Salt concrete/NaCl-solution. Black bars describe errors of 5 %.

Solid Salt concrete samples after 90 days test time are not investigated by x-ray diffraction yet. Maybe a change in phase composition correspondent to change in solution can be identified so that change in solution could be explained.

reached nearly its initial value after 45 days. Concentration of Ca in solution increased. This results from the dissolution of Salt concrete typical CSH-phases as a consequence of Mg-attack.

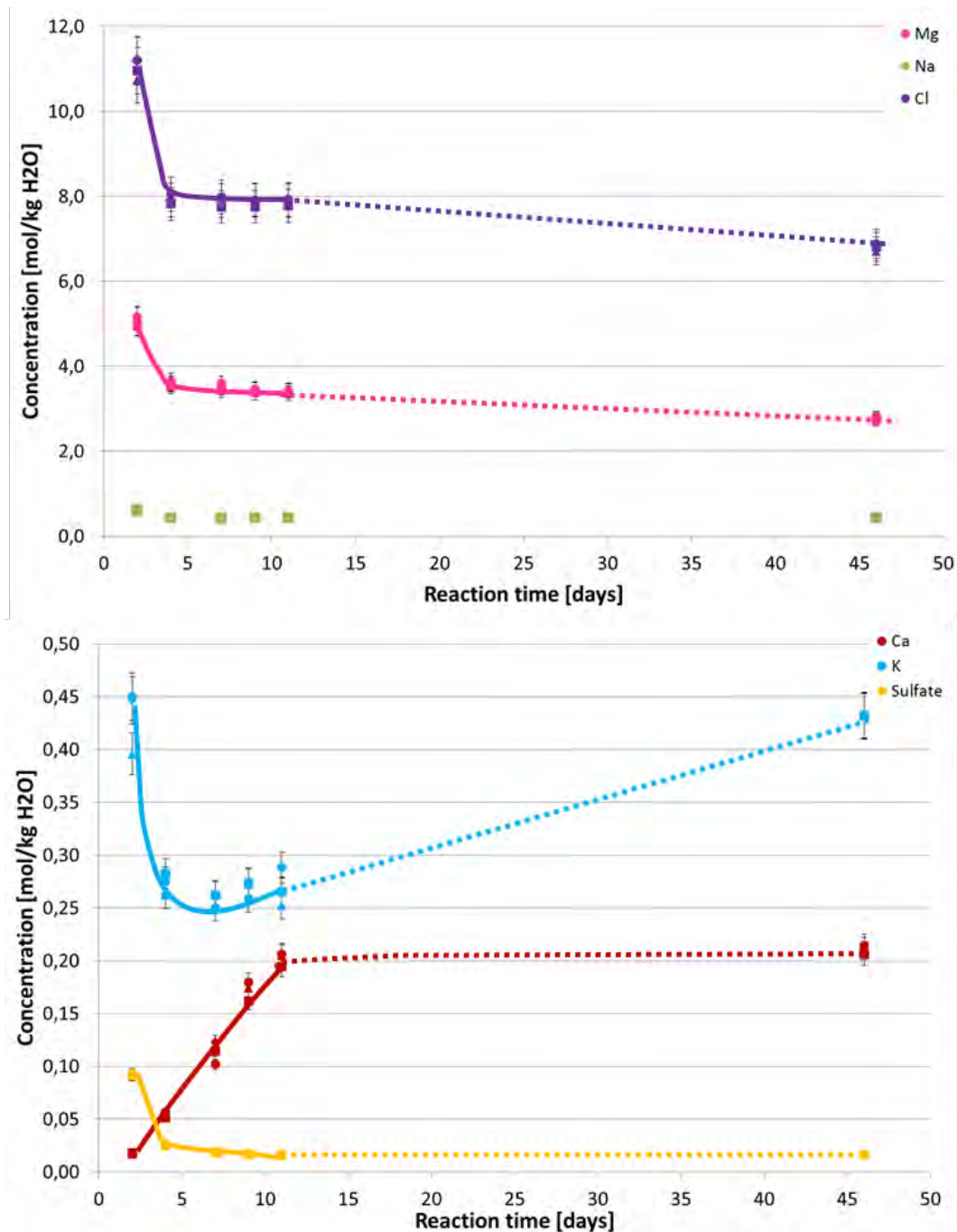


Fig. 6.10 Development of Mg, Na, Cl, Ca, K and sulphate concentrations in batch-experiments in the system Salt concrete/Mg-rich-solution. Black bars describe errors of 5 %.

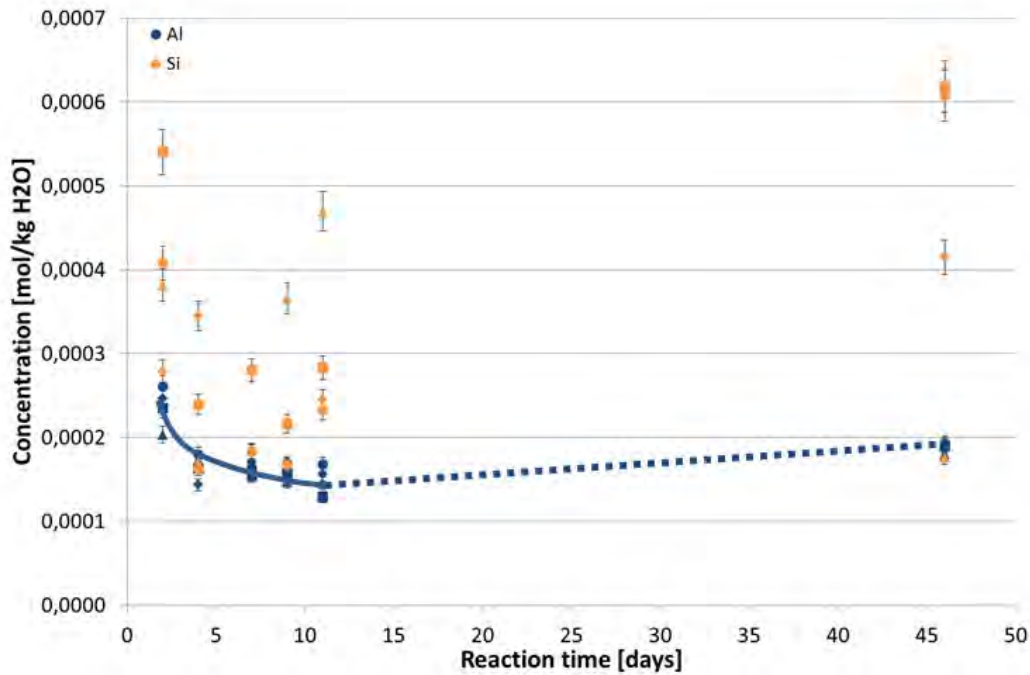


Fig. 6.11 Development of Al and Si concentrations in batch-experiments in the system Salt concrete/Mg-rich-solution. Black bars describe errors of 5 %.

Resulting from analyses of development of solution and solid phase composition following chemical processes could be assumed: Mg-, Cl, sulphate and K-concentrations decreased in solution in beginning of reaction. At the same time phases Brucite ($\text{Mg}(\text{OH})_2$), Gypsum ($\text{Ca}(\text{SO}_4) \cdot 2\text{H}_2\text{O}$), Bischofite ($\text{MgCl}_2 \cdot 6\text{H}_2\text{O}$), and Carnallite ($\text{KMgCl}_3 \cdot 6\text{H}_2\text{O}$) were formed. Concentrations of required elements in the solution decreased during formation of these phases (see Fig. 6.10). Only Ca-concentrations increased already in the beginning. Probably more Ca was dissolved by CSH-phase dissolution than was needed for formation of Gypsum or the precipitation of Gypsum is kinetic delayed. Anytime all CSH-phases were degraded and all sulphate was reacted. Consequently Ca-concentration in solutions became constant. Al concentration decreased in the beginning of experiments and increased with ongoing time again. Si concentrations varied during the batch-experiments. A significantly trend cannot determined. In batch-experiments it needed eleven days for the degradation of CSH-phases. Mg- and Cl-concentrations decreased furthermore during the continuing experiments. May be this occurs because of continuing generation of Brucite and Bischofite. A clear explanation for the increase of K-concentrations after seven days can currently not be given. May be dissolution of Carnallite is responsible. These are only assumptions be-

cause x-ray diffraction shows just a qualitative and not a quantitative analysis of phase composition.

6.1.5 Summary

Batch-experiments in the system Sorel concrete/NaCl-solution showed that the main reactions occur during 11 days. Within this time step no significant changes in solution composition were to identify. Solution changed during further experiment especially in its Cl and Na concentration. To which extent this circumstance is relevant to further corrosion process needs to be investigated.

By investigation of the system Sorel concrete/Mg-rich solution a generation of Bischofite and Carnallite was occupied which corresponds to the decrease of Mg, K and Cl concentrations in solution. If this processes result in a corrosion of Sorel concrete which is relevant for the long time stability of a sealing element is not clarified yet.

Experiments with Salt concrete in contact to NaCl-solution showed no significant changes in phase and solution composition. There were only small changes. Probably these changes results from dissolution of some phases in crushed salt, which was not in equilibrium with pure NaCl-solution (e. g. Polyhalite). But this dissolution should be very small because the main component of crushed salt is NaCl which is in equilibrium with the NaCl-solution.

Batch-experiments in the system Salt concrete/Mg-rich solution verified the expectation of corrosion of Salt concrete and dissolution of CSH-phases. The duration for cascade experiments according to the findings in the batch experiments were set to 11 days. Afterwards there are further reactions (for example the increase of K-concentration in solution) which need to be investigated.

Equilibration times determined with batch-experiments are only valid for systems with powdered concrete.

6.2 Cascade experiments (preliminary results)

Cascade experiments was executed on basis of results from batch-experiments (see section 6.1). With batch-experiments the duration of one cascade in each system was determined. In the system Sorel concrete/NaCl cascade experiments were executed with a cascade length of eleven days and in the system Salt concrete/Mg-rich-solution with a length of 15 days. Cascade experiments in systems Sorel concrete/Mg-rich-solution and Salt concrete/NaCl-solution was not executed at present. To which extent processes in those systems are relevant to the long term stability of sealing elements is investigated in diffusion and advection experiments.

It is acknowledged that the reaction times assigned to cascade experiments do not necessarily reflect the attainment of true thermodynamic equilibrium. Rather it is attempted to catch the main conversion in terms of solution and solid phase composition in a time frame which can be managed within a normal project life time. Cascade experiments reveal the most important solid phases to be accounted for in the thermodynamic database, and the difference between modelling and experimental results allows inferring on kinetic rate constants of dissolution and precipitation reactions.

6.2.1 Cascade experiments with Sorel concrete and NaCl-solution

Cascade experiments with Sorel concrete and NaCl-solution showed nearly constant increase of density of the solution from 1.196 to 1.219 g/cm³ (Fig. 6.12). It can also be assumed that in each cascade more elements dissolve.

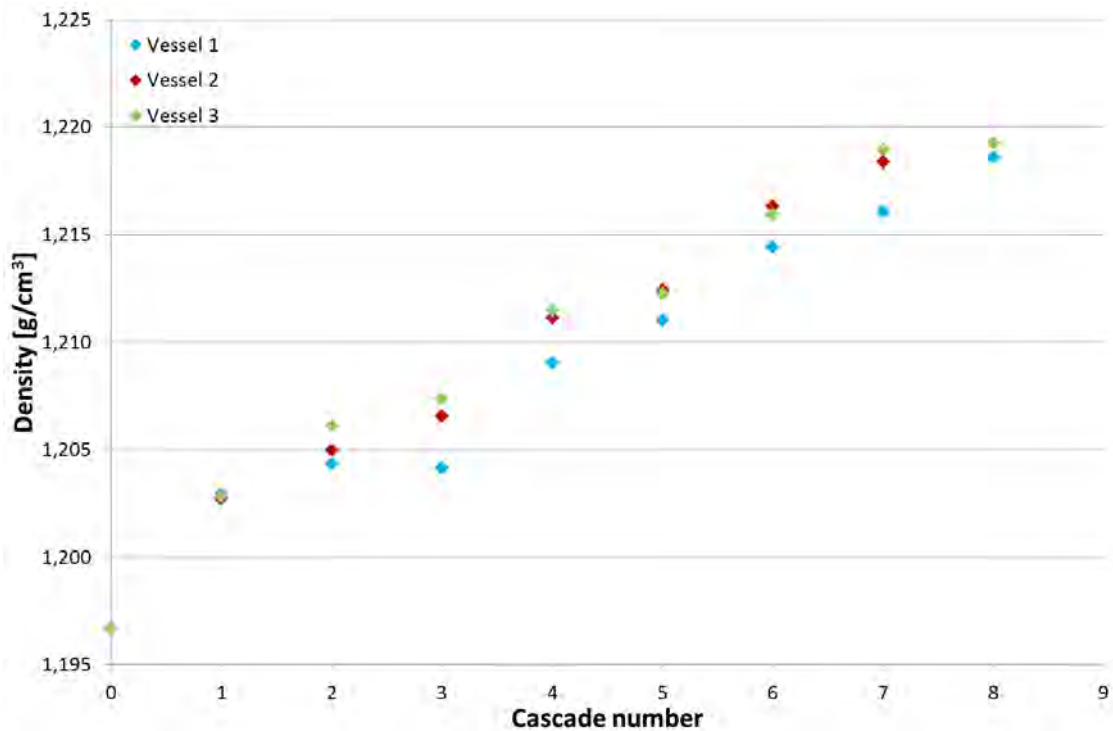


Fig. 6.12 Development of density in cascade experiment with Sorel concrete and NaCl-solution

Development of solution composition shows that Na and Cl concentrations was constant during the whole experiment (Fig. 6.13).

Concentrations of Ca decreased slowly and in parallel K concentration increased slowly. Mg concentration increased significantly and was six times higher in the end of cascade eight than in cascade one. The increase occurred nearly linear. Also sulphate concentration increased considerably and reached a final value which was about five times higher than in the beginning. Sulphate concentrations increased mainly in cascades one to five and more slowly in cascades six to eight. Probably the difference of sulphate concentrations in solution and solid phase become less and dissolutions of sulphate occurred more slowly now.

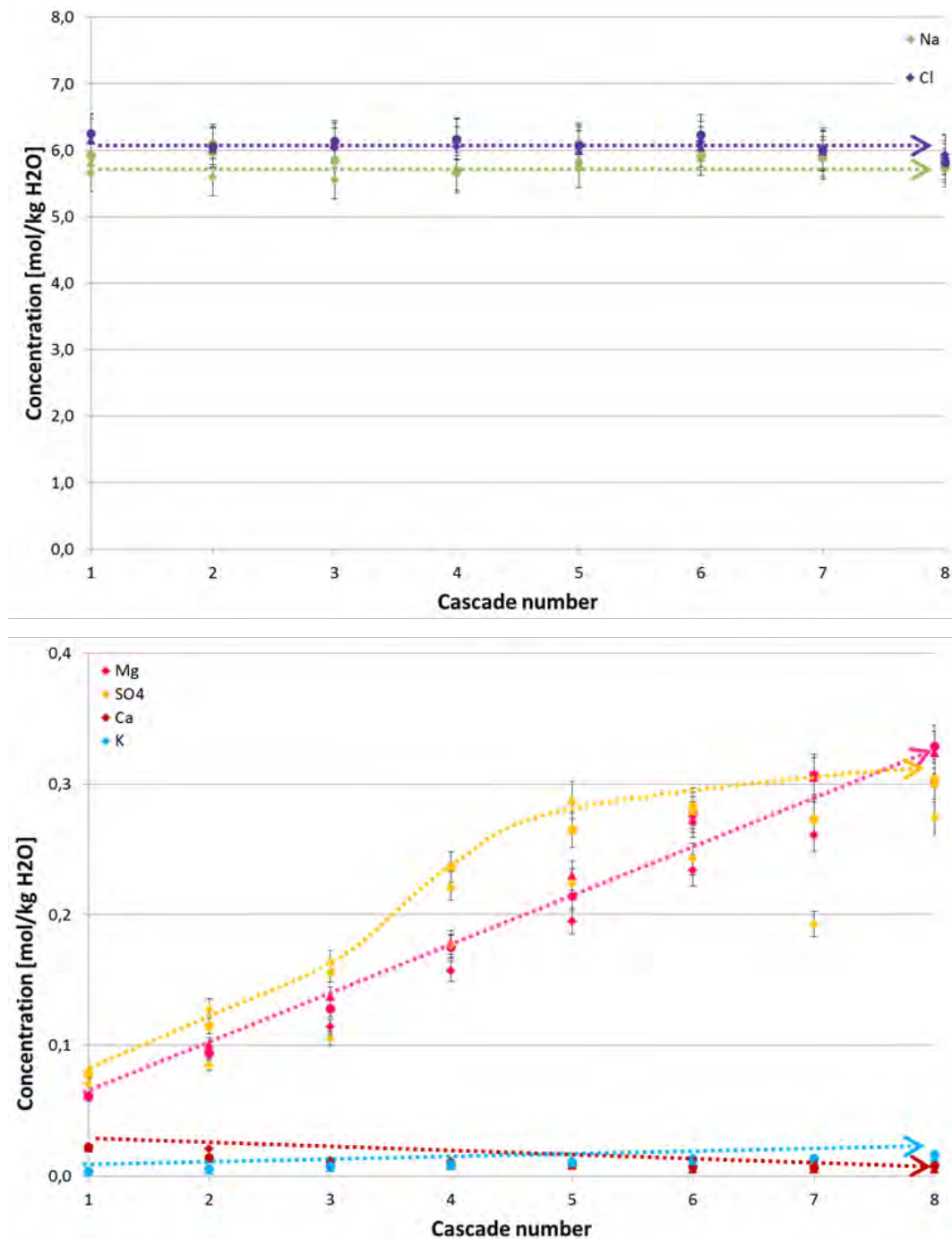


Fig. 6.13 Development of solution composition in cascade experiments with Sorel concrete and NaCl-solution. Black bars describe errors of 5 %.

Dissolution of 3-1-8-phase and of Anhydrite was to assume correspondent to x-ray-diffraction of batch-experiments. Increase of sulphate and Mg concentrations could be explained by that. Additionally Ca and Cl dissolved as constituents of 3-1-8-phase respectively Anhydrite but their concentrations did not increase in the solution. Hence it can also be speculated that new phases form when more concrete dissolve in NaCl-

solution compared with batch-experiments. For better interpretation of these reaction processes the x-ray-diffraction of concrete samples from cascade experiments still needs to be completed. Probably amorphous phases form which are not visible by x-ray-diffraction. In this case microscopically investigations are needed.

6.2.2 Cascade experiments with Salt concrete and Mg-rich-solution

Fig. 6.14 shows development of density in cascades one to six in the system Salt concrete and Mg-rich-solution. Density decreased in beginning of experiment (cascade 1) and increased with each cascade in further progress. Density of vessel 2, cascade 1 is probably deficient (a mistake by measuring of density was identified).

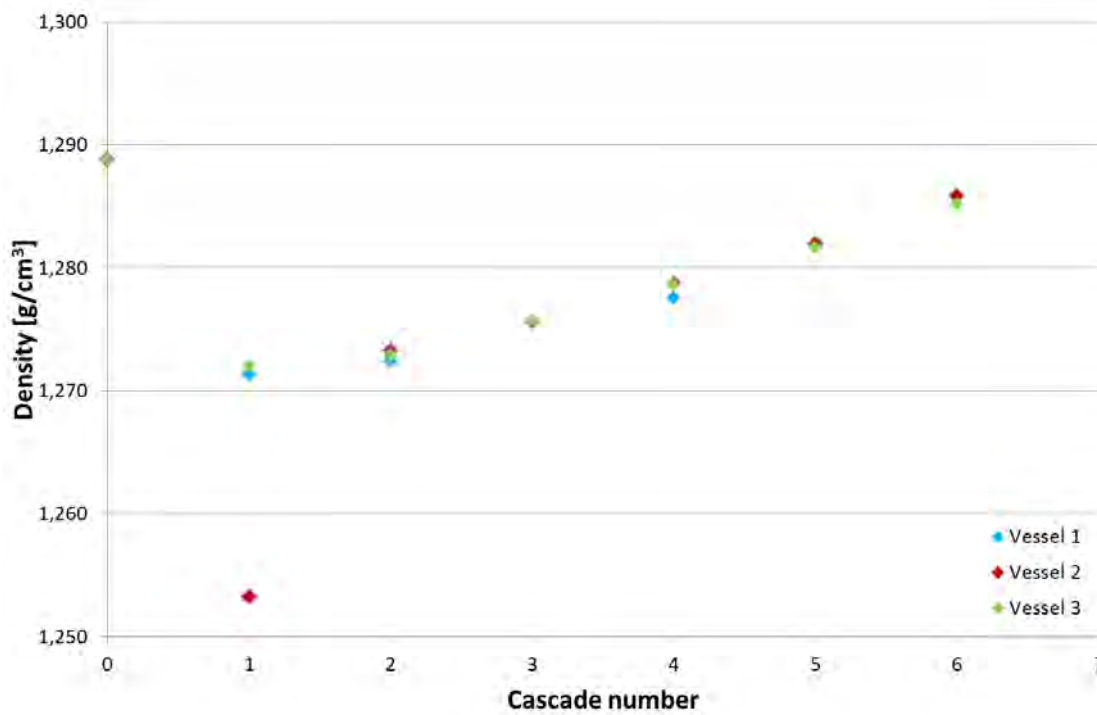


Fig. 6.14 Development of density in cascade experiment with Salt concrete and Mg-rich-solution

For further interpretation of density measurements analysis of solution and x-ray-diffraction of the Salt concrete samples of the cascade experiment needs to be awaited.

6.3 Diffusion experiments

Two types of diffusion experiments are executed (see section 5.3). It is assumed that diffusion-coefficients are between $1 \cdot 10^{-15}$ to $1 \cdot 10^{-13}$ m^2/s /HER 12/. In /MAT 12/ diffusion-coefficients for concrete of $1 \cdot 10^{-14}$ m^2/s are given. Consequently a maximal penetration of 0.01 m could be reached after 600 days of reaction, if a diffusion-coefficient of $1 \cdot 10^{-13}$ m^2/s and a permeability of the concrete between $1 \cdot 10^{-21}$ to $1 \cdot 10^{-21}$ m^2 is assumed (see Fig. 6.15).

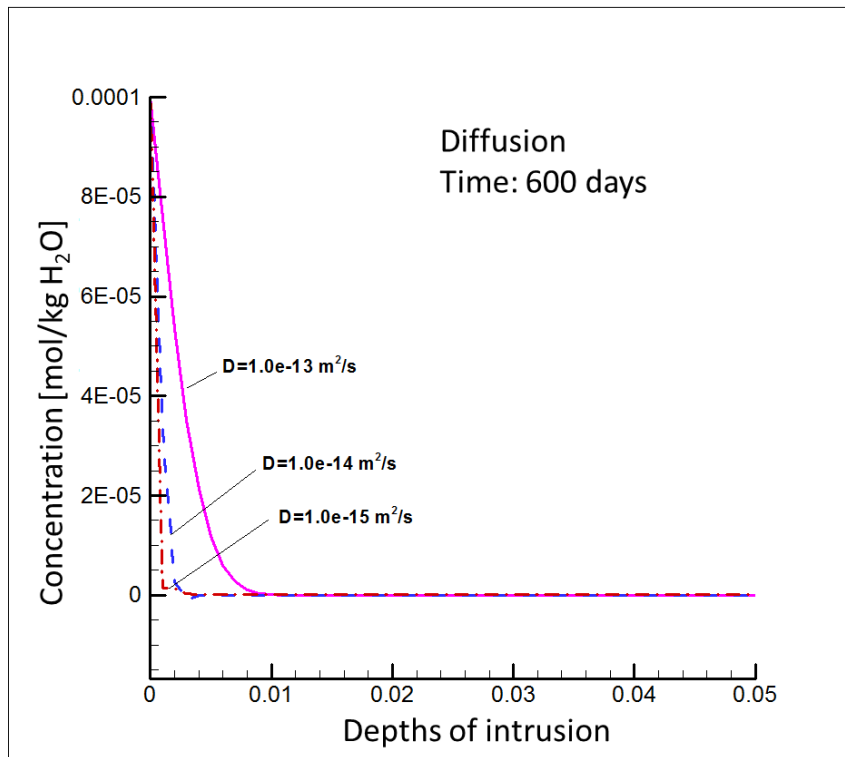


Fig. 6.15 Calculated penetration profiles by diffusive transport in concrete. Matrix permeability: 10^{-20} to 10^{-21} m^2 . Diffusion coefficients of 10^{-13} , 10^{-14} and 10^{-15} m^2/s /HER 12/

6.3.1 Through-diffusion experiments (pilot test)

Through-diffusion experiments are executed in three phases. In the first phase the samples was pre-saturated with unspiked solution. Samples of Salt concrete and of Sorrel concrete were placed in a gas-tight box (CO_2 -elimination) filled with NaCl- respectively Mg-rich-solution. Samples in the pilot tests had various lengths of 1 cm, 2 cm and 3 cm to determine if the sample length has an impact on the cumulative flux of tracer.

Ideally this is not the case. An increasing flux with decreasing sample length, however, indicates that diffusional transport is dominated by interfaces between bulk components of the matrix, such as salt- and cement grains and are therefore not representative for a large body of sealing material.

During pre-saturation the electrical conductivity was measured in regular time steps. The assumption is that samples are saturated if an electrical conductivity is measurable or increases rapidly. In Sorel concrete it needed about eight weeks until an electrical conductivity in 1 cm sample with Mg-rich-solution was measurable. After four month an electrical conductivity was also measurable in all other samples in both solutions. An electrical conductivity was not measurable in any Salt concrete samples after ten months. This reflects the extremely low permeability of this material. Consequently Salt concrete samples are still in phase one for saturation of samples.



Fig. 6.16 Samples in first phase of through-diffusion experiments before solutions were admitted. Sorel concrete (left) and Salt concrete (right)

Pre-saturated Sorel concrete samples were placed in diffusion-cells. In this phase non-spiked solution circulates at the bottom and at the top of the cells. In this phase, for which two times more time was spent than for the pre-saturation phase, it was assumed, that the sample fully equilibrates with the background, unspiked solution.

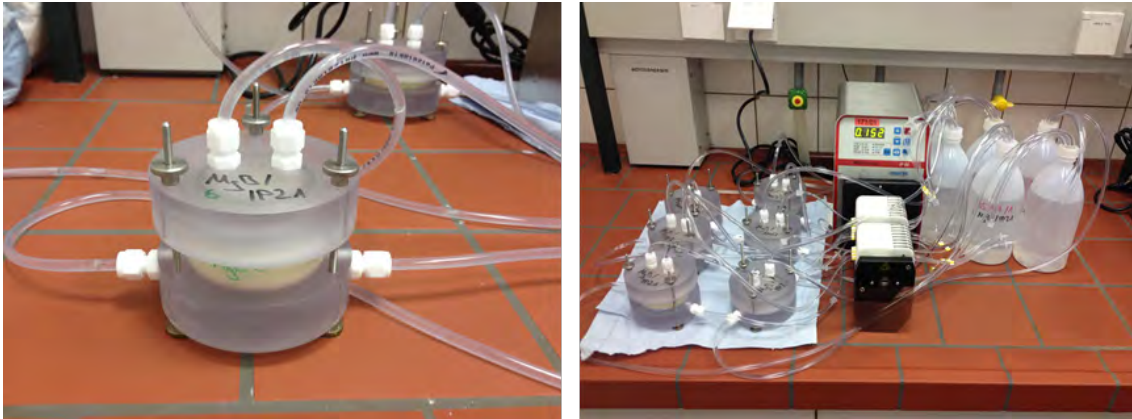


Fig. 6.17 Diffusion cell with inserted sample (left) and layout of through-diffusion experiments during phase 2 of experiment (right)

In the third phase the solution at the bottom of the diffusion cells was changed to a tracer spiked solution. The solution which was spiked with caesium and lithium was circulated at the bottom of the sample. The solution at the top of the sample only passed the sample and was afterwards collected in vessels. Over time it is assumed that a stationary flux evolves across the sample which is indicated by a linear plot of cumulated mass of tracer vs. time. Vessels were substituted twice a week and the tracer concentrations were determined by ICP-MS. Afterwards the cumulated mass of tracer was calculated.

Fig. 6.18 and Fig. 6.19 show that velocity of diffusion depends apparently on the sample length. In 1 cm samples diffusion occurs considerable faster than in the 2 cm and 3 cm samples. As explained above this phenomenon results from the inhomogeneity of Sorel concrete and diffusive transport occurs faster along the grain boundaries. Hence diffusion can occur very fast along grain boundaries in small samples and is not retarded by diffusion in the cement matrix. With increasing sample length percentage of diffusion in the cement matrix increases and consequently the whole diffusion process is slower.

In comparison the diffusion of caesium appears to be faster than for lithium.

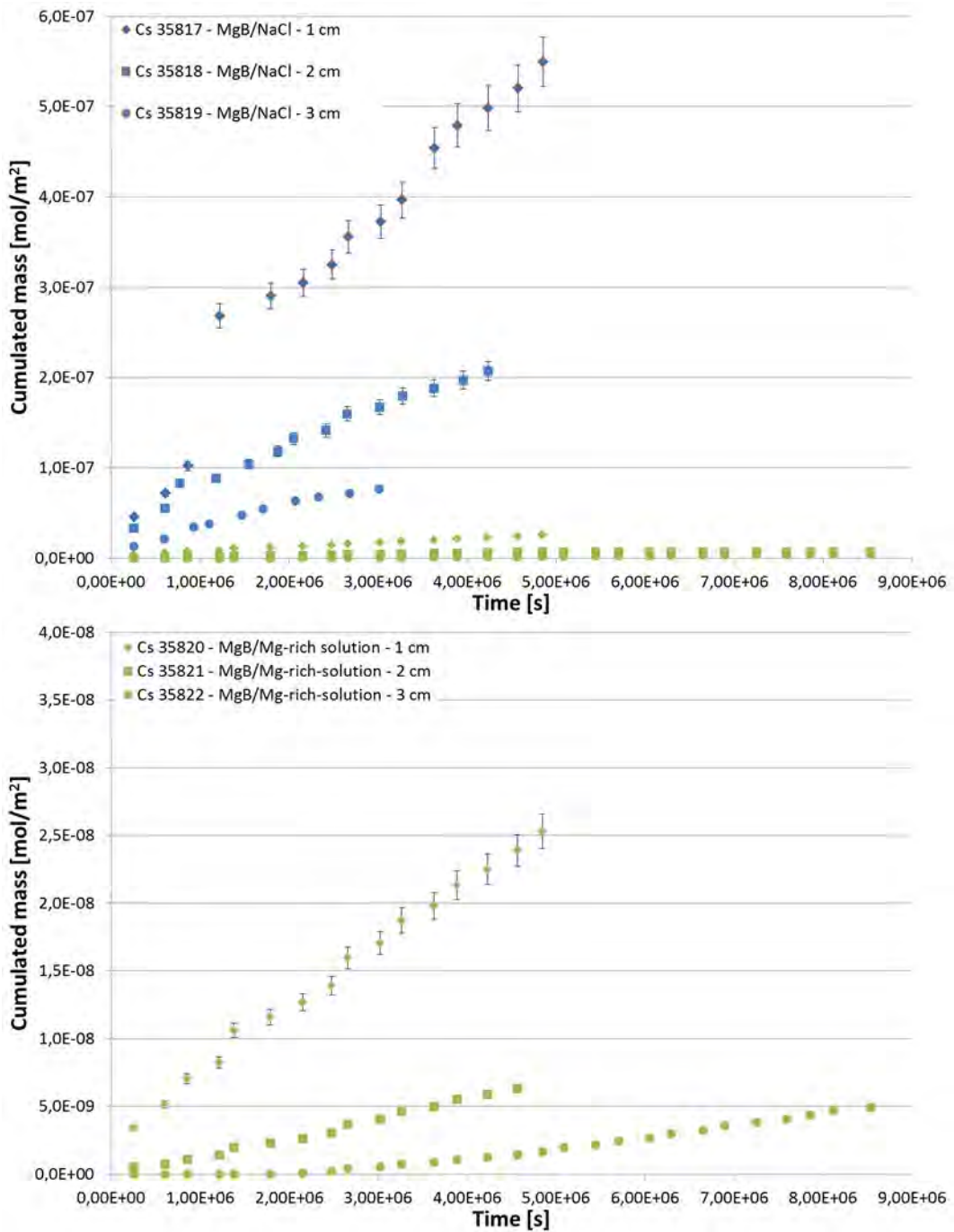


Fig. 6.18 Upper diagram: Cumulated mass of tracer lithium in diffusion experiments with Sorel concrete and NaCl-solution (blue) and Sorel concrete and Mg-rich-solution (green). Diagram below: Cumulated mass of tracer lithium (smaller scaling of y-axis). Black bars describe errors of 5 %.

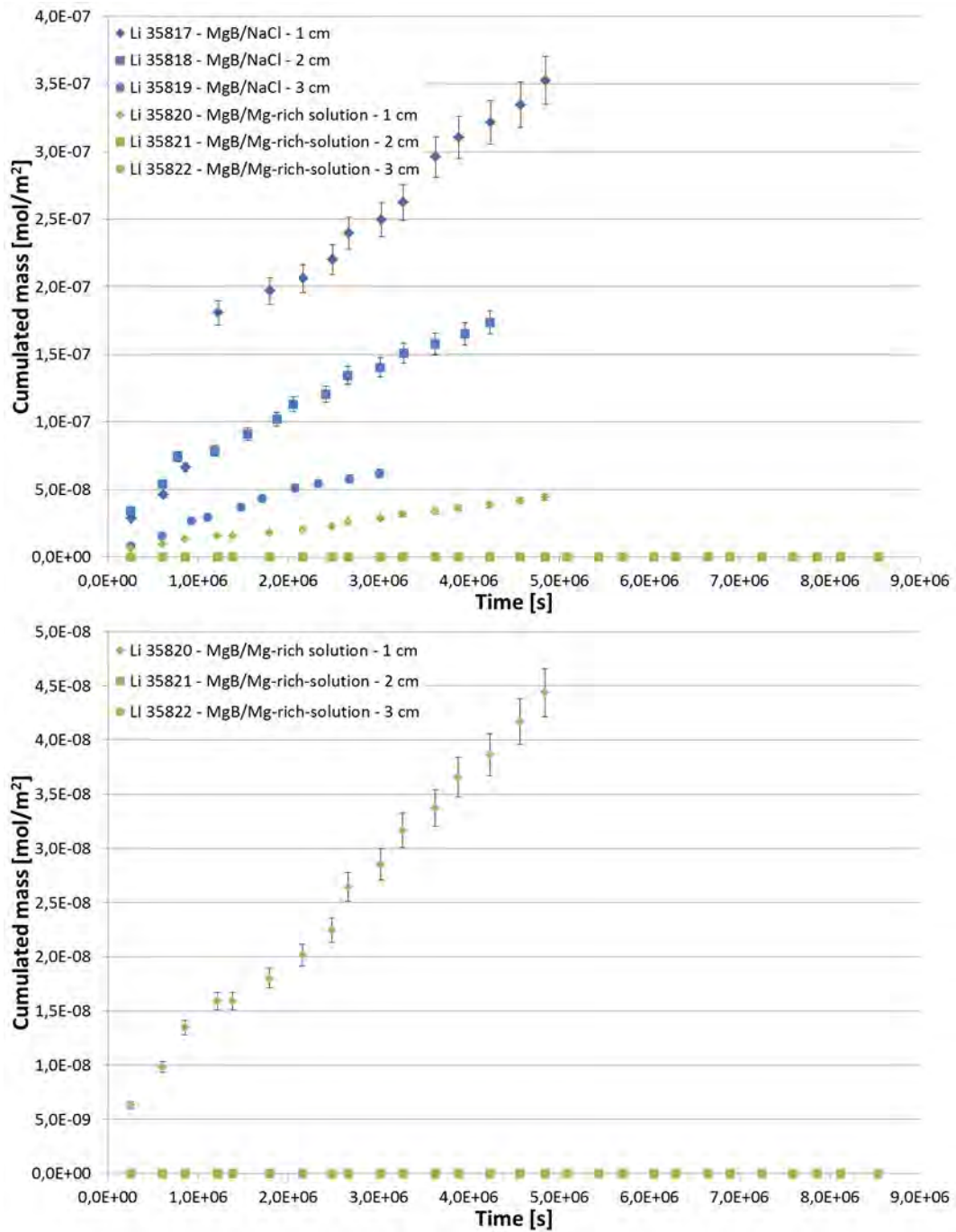


Fig. 6.19 Upper Diagram: Cumulated mass of tracer caesium in diffusion experiments with Sorel concrete and NaCl-solution (blue) and Sorel concrete and Mg-rich-solution (green). Diagram below: Cumulated mass of tracer caesium (smaller scaling of y-axis). Black bars describe errors of 5 %.

6.4 Advection experiments

6.4.1 Sorel concrete in contact with NaCl- solution

Advection experiments with Sorel concrete in contact with NaCl-solution were executed in two steps: In the beginning all samples were loaded with an injection pressure of solution of 20 bar. In this phase corrosion and its effects to permeability and porosity was investigated. In a second part kinetic effects have been investigated: the flow in three samples was interrupted for a while so that solution and concrete had more time to react. Afterwards the change of solution composition and permeability was investigated in the same manner as before. The stop of flow for samples AS 31-2, AS 32-5 and AS 34-1 is marked by vertical lines in Fig. 6.20.

Sorel concrete in contact with NaCl-solution was very quickly permeable to solution. Permeability was measurable in all samples after seven to sixty days and permeability increased constantly in all samples. Permeability around $1 \cdot 10^{-17} \text{ m}^2$ was reached in samples AS 31-1, AS 34-2 and AS 36-1 after a solution volume of about 250 ml passed the samples. It increased by a magnitude of a half to one. Permeability of samples AS 32-5 and AS 34-1 was less - at around $5 \cdot 10^{-18} \text{ m}^2$ - after a flow volume of 250 ml solution. Core AS 31-2 had the lowest initial permeability but the highest permeability increase proportional to volume of passed through solution. Permeability increased over one magnitude. Permeability increased to $1 \cdot 10^{-18} \text{ m}^2$ after 60 ml of NaCl-solution passed the sample. Afterwards, permeability increased slower.

Results from first part of advection experiments show that permeability increased in all samples but development seems to stop at values below $1 \cdot 10^{-17} \text{ m}^2$. Probably solution passed samples faster than reactions occur. Hence in three samples flow was interrupted and solution remained in the samples for a while. The expectation of further corrosion processes was confirmed by the stepwise increase of permeability. Expectation of receiving a stepwise increase of permeability was reached (see Fig. 6.20). After each interruption of flow through (marked by vertical lines) an increase of permeability was measurable. This circumstance confirms earlier assumption that solutions passed the samples too fast for further effects of corrosion.

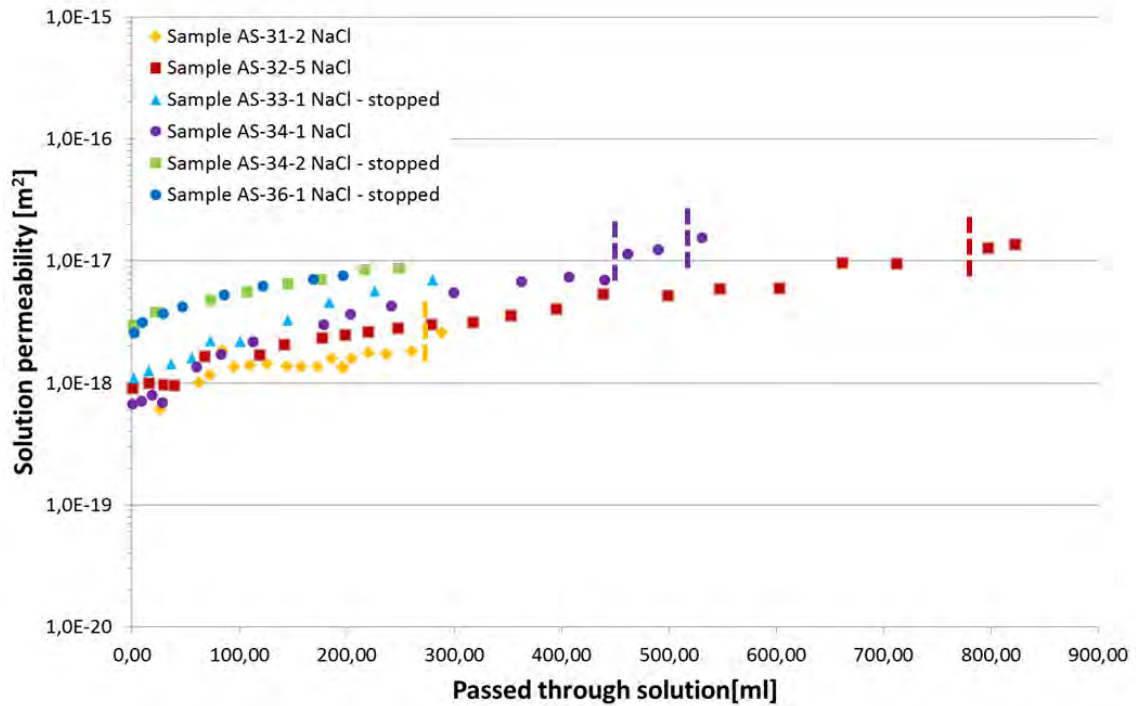


Fig. 6.20 Development of permeability of Sorel concrete samples in contact to NaCl-solution (vertical lines mark time steps in which flow through of solution has been stopped, further reaction between concrete and solution has been awaited and afterwards change of permeability and solution composition was investigated)

Results of analysis of solution composition showed (Fig. 6.21) that sulphate, magnesium and potassium concentrations are high in the beginning of advection experiments. But concentrations decreased quickly around 80 to 90 % after circa 25 ml solutions had flowed through the sample. Concentrations of calcium increased along with a decrease of Mg, K, and sulphate. Afterwards potassium concentrations decreased slowly with ongoing experiments.

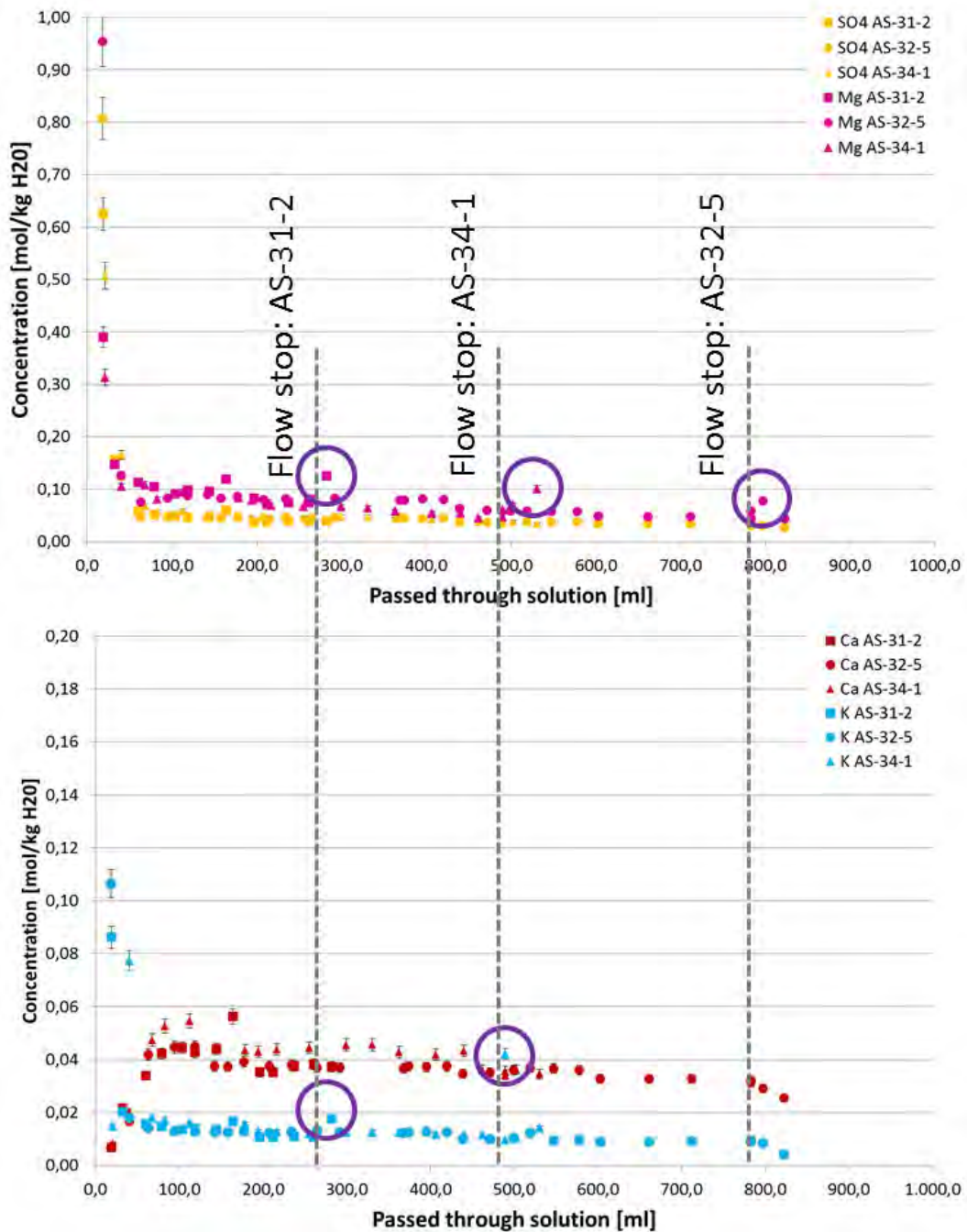


Fig. 6.21 Development of solution composition in advection experiments with NaCl-solution. Circled points mark measurements after stop of flow through of solution. Black bars describe errors of 5 %.

The second part of advection experiments showed additionally that it is important to take very small volumes of solution after an interruption of flow to verify change in solution composition. Some volumes were too big and so differences in concentration were not measurable anymore because the small mass of reacted solution was diluted by non-reacted solution. Results of solution analysis showed that magnesium and potas-

sium may dissolve further if reaction time was increased (marked by the violet circlets in Fig. 6.21). An increase of potassium concentrations was detectable in sample AS 31-2 and AS 34-1. The reason why an increase of potassium was not detectable in all samples is currently unknown.

In general advection experiments showed that NaCl-solution corrodes Sorel concrete and corrosion results in an increase of permeability. The corrosion process is influenced by kinetic effects.

6.4.2 Sorel concrete in contact with Mg-rich solution

Fig. 6.22 shows the development of permeability of Sorel concrete in contact with Mg-rich-solution. This experiment was executed in parallel to the experiment with NaCl-solution so that samples were exposed at the same time to potential attack by solution. Permeability is around $1\text{-}5 \cdot 10^{-19} \text{ m}^2$ in AS 31-8 and AS 32-4 and was measurable after 200 to 250 days. Permeability for AS 31-4 and AS 32-2 is a bit smaller and was measurable after 350 to 400 days. Sample AS 32-1 has the lowest permeability of $2,28 \cdot 10^{-19} \text{ m}^2$ and was measurable after 420 days. In sample AS 36-2 permeability was already detectable after 50 days. The value was constant at $5 \cdot 10^{-19} \text{ m}^2$ over 250 days. Then permeability increased suddenly up to $8 \cdot 10^{-17} \text{ m}^2$ after circa 170 ml of passed through solution. It decreased in the meantime to initial permeability again and increased afterwards significantly over one and a half magnitude.

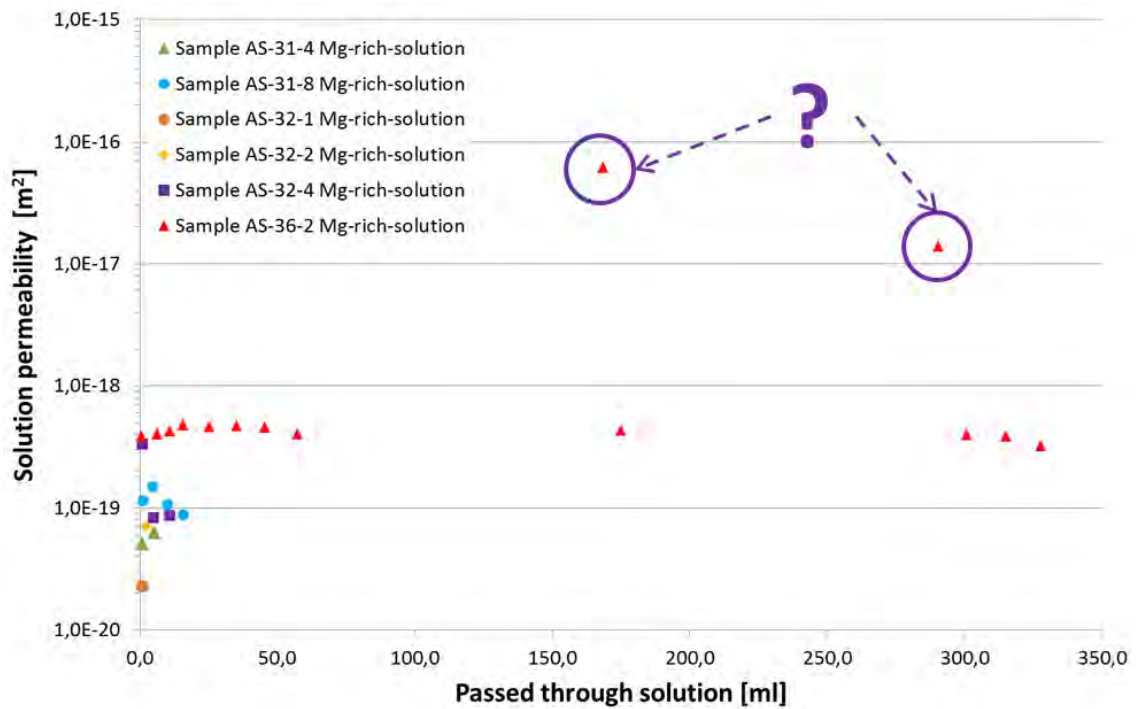


Fig. 6.22 Development of permeability of Sorel concrete samples in contact to Mg-rich-solution. The reason for higher values of permeability of sample AS-36-2 (marked by the interrogation mark) is not clarified yet.

Analysis of solution is currently only available for AS-36-2. Results showed that there is a pronounced decrease of sulphate concentrations of solution and also a decrease of potassium concentrations. Concentrations of calcium and magnesium did not change.

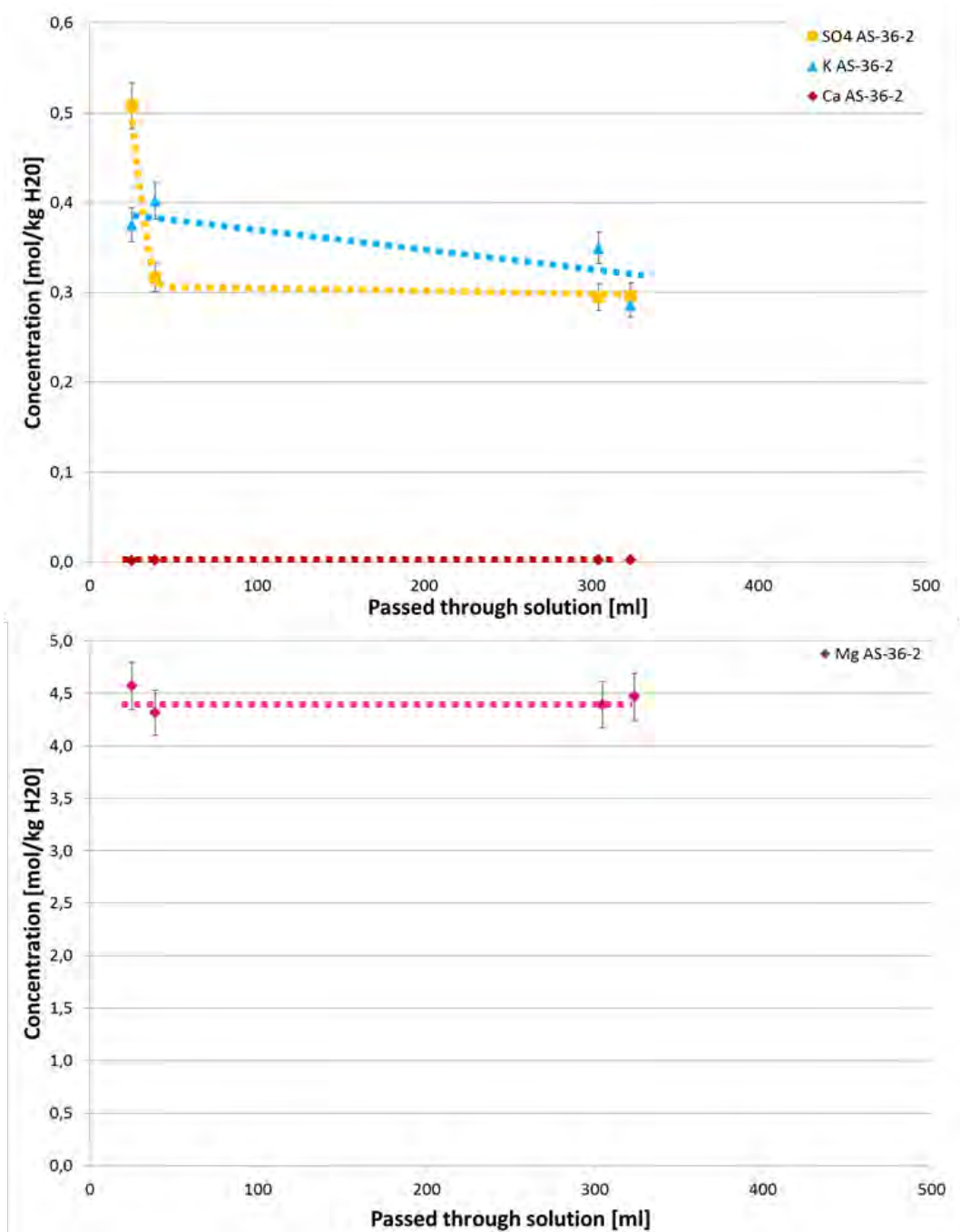


Fig. 6.23 Development of solution composition in advection experiments with Mg-rich-solution

6.4.3 Salt concrete – Gas permeability

Measurements of the permeability of Salt concrete to gas showed that Salt concrete has a very small or no permeability to gas. Permeability to gas was not measurable in 80 % of the samples, when a confining pressure of 5 MPa was reached (simulating the

initial stress conditions at core sample retrieval). Permeability to solution is estimated one order smaller than permeability to gas. Hence experiments for investigations of permeability to solutions are not executed on Salt concrete without a contact zone.

6.4.4 Summary

Results from advection experiments confirm that Sorel concrete is not stable against NaCl-solutions which is known from former investigations. Corrosion occurs by the dissolution of 3-1-8 phases, which results in an increase of porosity and consequently permeability. X-ray diffraction of the Sorel concrete from batch-experiments showed this process of sorel phase dissolution well (see Fig. 6.1 and Fig. 6.2). In a next step secondary phases need to be identified.

Investigations of Sorel concrete in contact with Mg-rich-solution showed a much better resistance. But contrary to earlier investigations and according to new batch-experiments the corrosion of Sorel concrete cannot be excluded completely because of the development of permeability. One hypothesis is that the flux in advection experiments results from connected pore spaces so that Mg-rich-solution flows very slowly through the samples under injection pressure without corrosion. Constant permeability in AS 31-8 and AS 34-1 argues for it. It should also be considered that very slow corrosion processes may occur because of the permeability increase in AS 36-2. This hypothesis is supported by results from batch-experiments and the change of concentration of sulphate and potassium in analysed solution. Probably there are also corrosion processes in this system. It needs to be investigated if these influence the long-time sealing capacity of a Sorel concrete sealing element significantly.

6.4.5 Combined sample Sorel concrete/rock salt in contact with Mg-rich-solution

The combined sample of Sorel concrete/rock salt was produced as described in section 5.4. The sample was coated with a rubber jacket and placed in an isostatic cell equipped with hydraulic lines to allow for axial flow-through of gas or liquid and determination of the system permeability. A photo of a coated sample and the cell arrangement are shown in Fig. 6.24.



Fig. 6.24 Coated sample in an isostatic cell (left) and cell arrangement (right)

At the beginning of the test permeability to gas was measured while confining pressure was increased stepwise up to 5 MPa. Permeability was around $2 \cdot 10^{-14}$ to $3 \cdot 10^{-13} \text{ m}^2$. Increase of confining pressure showed less influence to development of permeability to gas. In the next step the sample was loaded with an injection pressure of Mg-rich-solution at one end face. Permeability was circa $1 \cdot 10^{-14} \text{ m}^2$ in the beginning and increased quickly over one magnitude to $1 \cdot 10^{-13} \text{ m}^2$. Increase of confining pressure from 3 MPa to 5 MPa showed no significant influence to permeability. When confining pressure was increased to 7 MPa a small decrease of permeability could be identified. But further increases of confining pressure showed no influence to development of permeability. Permeability reached finally values of $5 \cdot 10^{-13} \text{ m}^2$. At this point the experiment was stopped and the sample was dismantled from the isostatic cell.

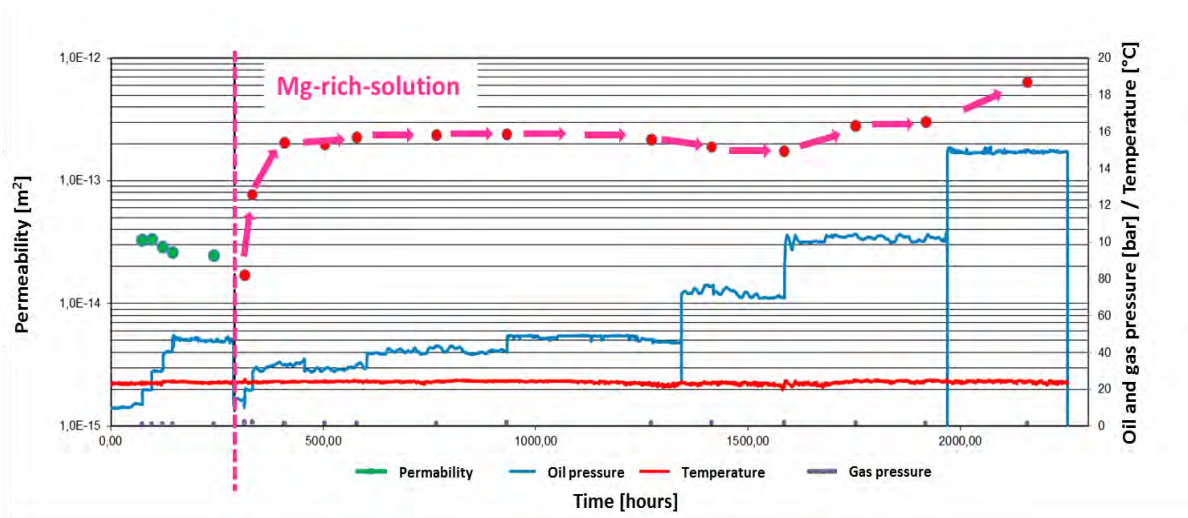


Fig. 6.25 Work curve: Development of permeability of a combined sample (Sorel concrete/rock salt). Permeability increases directly after start of flowing through with Mg-rich-solution.

After reconstruction significantly gap could be identified at both end faces. Fig. 6.26 shows scans from inflowing and outflowing face of the sample. The crack at the inflowing face is bigger compared to the crack at the outflowing face. Labeling of the samples shows also that the crack developed nearly in a straight line between both end faces. Hence high permeability of this combined sample results from the developed crack at the contact zone between Sorel concrete core and rock salt. Against expectations a compaction and minimizing of contact zone was not possible. It remains to be clarified, if the process of developing a flow path results from corrosion of Sorel concrete or from dissolution of rock salt, if Mg-rich-solution is not in equilibrium with it.

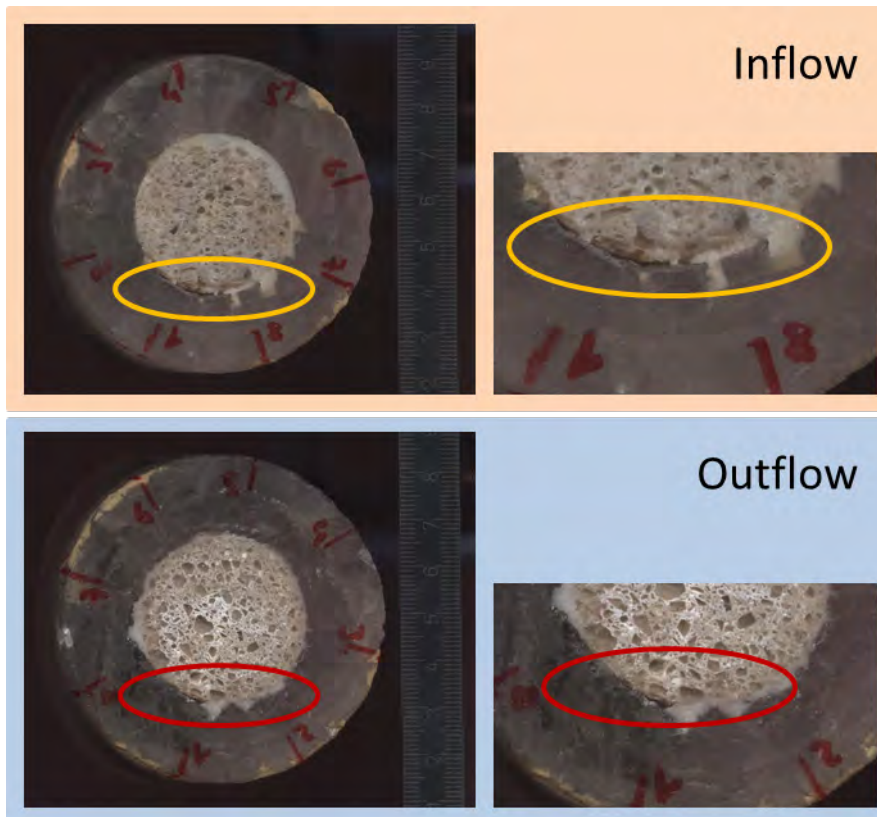


Fig. 6.26 Combined sample (Sorel concrete/rock salt) after flowing through with Mg-rich-solution. At the contact zone is clearly a crack to identify

6.4.6 Combined sample Salt concrete/rock salt in contact with NaCl-solution

The next experiment described follows the same preparation as the experiment with Sorel concrete. The combined sample of Salt concrete/rock salt was prepared in the same manner as before and placed in the isostatic cell. In the beginning the sample was loaded with a confining pressure of 1 MPa which was increased stepwise up to

10 MPa. A significant influence to development of permeability to gas could not be detected. Gas-permeability was around $2 \cdot 10^{-14}$ to $3 \cdot 10^{-14}$ m². Because we did not succeed to reduce the permeability by exerting a radial pressure of up to 10 MPa the sample was subsequently subjected to NaCl-solution. After an initial flow of solution the contact zone closed up in a time period of two months. Before sample was loaded with an injection pressure confining pressure was reduced to 1 MPa. Permeability to NaCl-solution was $1 \cdot 10^{-14}$ m² in the beginning and decreased continuously over five magnitudes within 40 days. After 60 days no flux was measurable anymore.

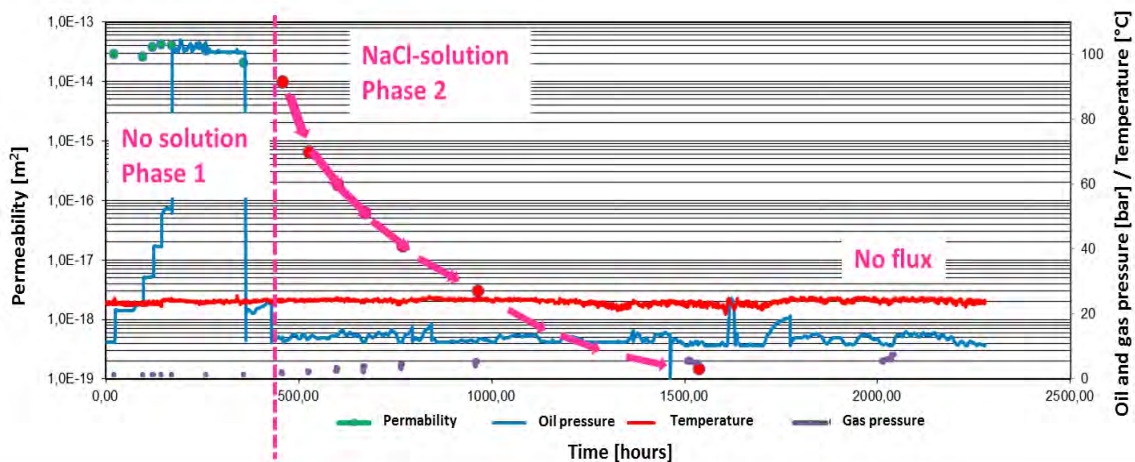


Fig. 6.27 Work curve: Development of permeability of a combined sample (Salt concrete/rock salt). Phase 1: Compaction of sample without solution – no significant decrease of permeability to gas. Phase 2: Flowing through of NaCl-solution with a very small surrounding pressure – clearly decrease of permeability to solution

Arrangement of this experiment showed that a confining stress up to 10 MPa did not result in a fast closure of the contact zone between a sealing element of Salt concrete and the surrounding rock salt. But presence of NaCl-solution and a small confining pressure of 1 MPa resulted very quickly in a closure of contact zone. Currently it is not clarified if reduction of permeability results from mechanical closure by creeping of salt, which is accelerated in the presence of solution, or by chemical reactions. Probably a combination of both processes is responsible for it.

6.4.7 Combined sample Salt concrete/rock salt in contact with NaCl- and Mg-rich solution

Further experiment was performed with a combined sample, which percolated with NaCl-solution in the beginning (similar to the experiment shown before). After the contact zone was closed up to a certain permeability the solution was changed to a Mg-rich-solution. Fig. 6.28 shows the measuring results from this type of advection experiment. At the beginning of the experiment permeability of the combined sample was reduced by a confining pressure and flow through of NaCl-solution (phase 1, not depicted). After solution was changed to Mg-rich-solution, permeability suddenly increased by two orders of magnitude and decreased by one order of magnitude when injection pressure was reduced. After two month of contact with Mg-rich-solution the permeability started to increase again. This phenomenon results from chemical processes in Salt concrete as former investigations at GRS have shown.

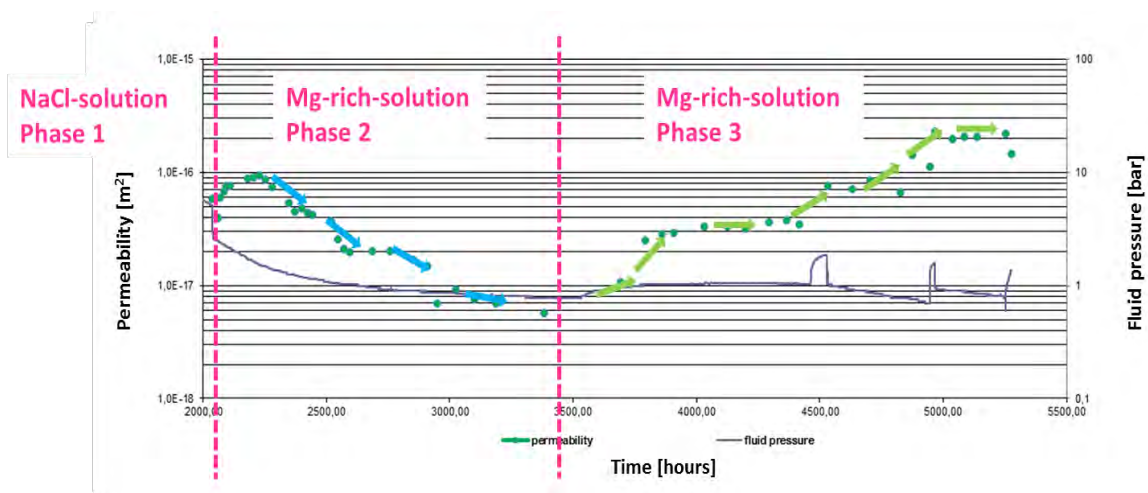


Fig. 6.28 Development of permeability of a combined sample (Salt concrete/rock salt). Phase 1: Flow of NaCl-solution and compaction of sample. Phase 2: Change to Mg-rich-solution and decrease of permeability. Phase 3: Increase of permeability

It is assumed that the high injection pressure in beginning of phase 2 generated the increase of permeability. Maybe chemical processes could not proceed because solution passed the sample faster than processes needed to proceed. After injection pressure was reduced, chemical processes could proceed. When the Mg-rich-solution is brought in contact with Salt concrete, free hydroxide (OH^-) is fixed by magnesium and Brucite ($\text{Mg}(\text{OH})_2$) is precipitated. Now pores are clogged by Brucite and the pH de-

creases to 8-9 (phase 2). As a result of the pH decrease Portlandite ($\text{CaOH})_2$ becomes instable and decomposes in Ca- and hydroxide ions. After consumption of all Portlandite the pH decreases further and stabilizing CSH-phases are dissolved. Now concrete loses its stability and permeability starts to increase (phase 3) /NIE 14/. Hence, the dissolution of CSH-phases can also be assumed in this experiment on the basis of increasing permeability and the knowledge of corrosion process of Salt concrete in contact with Mg-rich-solution. Compared with batch-and cascade- experiments dissolution needs more time because of the smaller specific surface of solid samples.

6.4.8 Summary

Advection experiments on Salt concrete showed that presence of NaCl-solution could result in a complete closure of contact zone. If the contact zone is not closed completely Mg-rich-solutions lead to a corrosion of Salt concrete as described and the sealing element loses its sealing function. A further question is if an increase of permeability also can be reached after a complete closure of the contact zone as in first experiment of Salt concrete/rock salt. This circumstance will be investigated in the LAVA-2 project.

7 Description of the state of the art of related chemical process modelling

In general, the chemical corrosion mechanisms in Salt concrete are the same for the diffusive and advective reactive transport process. A model for the diffusive and advective corrosion processes of Salt concrete in contact with the corrosive Mg-, SO₄- and Cl-rich brine are shown schematically in Fig. 7.1. The left part of the figure shows the diffusion controlled corrosion process in the undisturbed concrete matrix. On the right the corrosion on cracks is illustrated.



Fig. 7.1 Schematic representation of the chemical corrosion processes in Salt concrete due to the interaction with Mg-, SO₄- and Cl-rich salt solutions (left) diffusive matrix corrosion, (right) advective matrix corrosion on cracks (in /HAS 03/ modified after /BON 92/)

If a Mg- and SO₄-rich salt solution attacks Salt concrete first Brucite (Mg(OH)₂) will be formed at the surface of the cement structure. This leads to a mass flux of OH⁻ from the matrix towards the exterior of the structure and to a SO₄²⁻ flux from the intruding solution into the matrix. Due to the depletion of OH⁻ ions in the concrete CSH phases will be dissolved. The released Ca²⁺ reacts with the SO₄²⁻ to precipitate as Gypsum (Fig. 7.1). The crystallization pressure of the newly built phases can lead to the formation of cracks in the material structure.

After Portlandite (Ca(OH)₂) from the concrete matrix is exhausted the pore fluids are not buffered anymore and the pH decreases from about 13 to 9. The CSH phases in the concrete matrix become instable and will gradually disappear (Fig. 7.1).

If the diffusion of the OH⁻ from the concrete body towards the surface of the structure is not balanced by an appropriate formation of Brucite, (precipitation kinetics) Mg enters into the matrix and can form MSH phases. The Mg content in solution decreases con-

tinuously until Mg is consumed. The chemical processes have been observed in many experiments with cemented materials /SKA 02/ and could be reproduced by geochemical modelling for the system Salt concrete in contact to different brines /MEY 99/, /MEY 02/, /MEY 03a-c/, /MEY 04/.

The described reactions take place in the matrix of the concrete as well as on cracks and at the boundary of the concrete with the salt formation. The experiments showed that the formation of $Mg(OH)_2$ first leads to a decrease of permeability and the subsequent formation of MSH phases increases the permeability (s. Fig. 7.2).

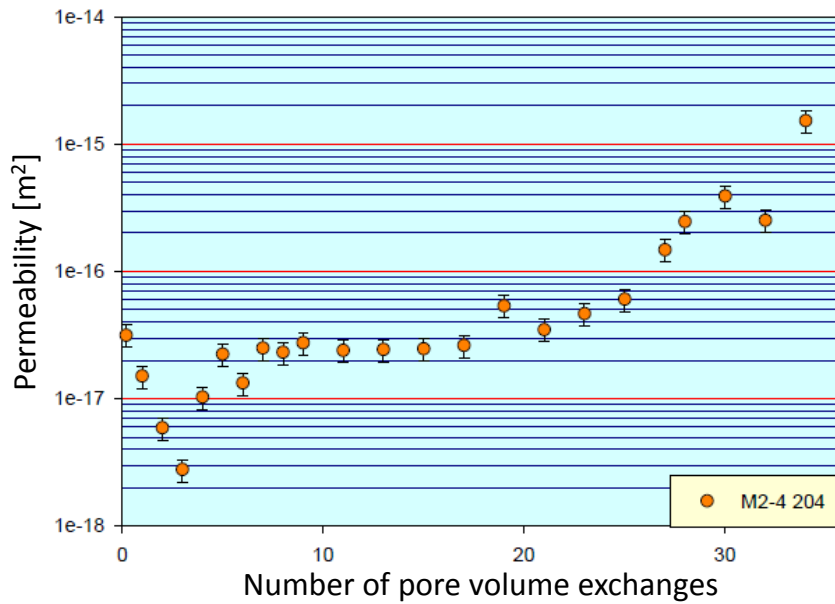


Fig. 7.2 Permeability changes of M2-4 Salt concrete in contact with IP21 solution at rising numbers of pore volume exchange /MEY 03b/

The chemical processes which are responsible for the corrosion are the same regardless of the corroding solution entering the sealing structure very slow (only driven by diffusion) or faster (driven by advection of the brine). But for the velocity of the corrosion and time dependence of permeability increase it is very important to know if the inflow of brine into the sealing structure is driven by a slow diffusion process or by much faster advection. For permeabilities lower than 10^{-18} m^2 the inflow of brine into the concrete structure becomes very slow. The actual initial permeabilities of fresh Salt concretes are in general considerably lower than 10^{-18} m^2 leading to flow velocities in the order of 10^{-8} m/a . This flow rate can be assumed in the undisturbed matrix without cracks. The corroding solution advances so slowly that the corrosion is controlled by diffusion only.

In addition, the corrosion velocity is dependent on the pore structure of the concrete. The corrosion advances faster the more pores are interlinked thus promoting mass exchange. The degree of interconnectedness of the pores depends largely on the initial water/cement ratio. Higher initial water/cement ratios in a concrete result in a higher initial porosity and permeability of the concrete.

The lower the initial water/cement ratio the faster the steadily progressive hydration leads to an interruption of the pore network (a "discontinuous pore structure"). This process is completed at w/c ratios of about 0.45 within a few days. For only slightly higher w/c ratios, however, this process requires months to years. In general, when w/c ratios are greater than 0.7 a discontinuity is never reached /POW 59/. Equally, a significant dependence of the porosity of the w/c ratio could be observed. The porosity increases with w/c ratios above 0.5 rapidly /HEA 99/, /POW 58/.

In the same context /KIN 68/ underlined, that in dense concretes the remaining pores are quickly clogged by secondary products, so that the diffusion of corrosive elements in the concrete matrix and thus the corrosion rate as a whole slowed down. /KAN 61/ studied the resistance of cement mixtures in contact to MgSO_4 solution. Cement mixtures with a very low water content (w/c = 0.23 - 0.26) behave largely resistant, while mixtures with w/c = 0.35 have lost half of their strength after two years.

Also /GJÖ 86/ (cit. in /MEH 91/) showed that in some cases less the chemical composition than the permeability of cement has a decisive impact on the corrosion rate. Even after an exposure time of 60 years, corrosion phenomena to only depths of about 5-7 mm could be detected at harbour piers.

For Sorel concrete Sglavo et al. showed that the hardening behaviour and mechanical strength of Sorel concrete strongly depends on two phases, $3\text{Mg}(\text{OH})_2 \cdot \text{MgCl}_2 \cdot 8\text{H}_2\text{O}$ and $5\text{Mg}(\text{OH})_2 \cdot \text{MgCl}_2 \cdot 8\text{H}_2\text{O}$, usually referred to 3-1-8- or 5-1-8 phases, respectively /SGL/GEN 11/. While at temperatures usually found under ambient conditions in underground repositories, thermodynamic equilibrium establishes with the 3-1-8-phase within a time frame of several months up to years at the latest, transformation kinetics, and hence the overall performance of a flow barrier made up with Sorel concrete, is strongly affected by the transient temperature regime during hardening and the initial reactivity of the MgO-component in the primary material /SGL/GEN 11/. As the hardening of Sorel concrete with MgCl_2 -solution is exothermal, transient temperatures within

the barrier can be as high as 120°C /DIN/FRE 10/. Thus, earlier results about the reactivity of Sorel concrete must be re-evaluated focussing on the temperature regime applied during their fabrication.

To make things more complicate, yet another phase – 9-1-4 ($9\text{Mg}(\text{OH})_2 \cdot \text{MgCl}_2 \cdot 4\text{H}_2\text{O}$) – had been identified, being formed intermediately /DIN/FRE 10/. Under the impact of higher temperatures the 3-1-8 phase may be dehydrated to lower hydrates, identified as the phases $3\text{Mg}(\text{OH})_2 \cdot \text{MgCl}_2 \cdot 5.4\text{H}_2\text{O}$ and $3\text{Mg}(\text{OH})_2 \cdot \text{MgCl}_2 \cdot 4.6\text{H}_2\text{O}$ /RUN/DIN 14/. Furthermore, during the hardening process Sorel concrete is subject to reaction with CO_2 present in the atmosphere, leading to the formation of carbonate phases within the matrix.

To obtain reliable results which can be closely associated with specific points within a flow barrier after a given time of hardening, experiments on the reactivity of hardened Sorel concrete need to be conducted under defined temperature conditions, thereby excluding CO_2 .

As with Salt concrete, the chemical corrosion mechanisms are the same for the diffusive and advective reactive transport process. With Anhydrite present in the rock salt from which the intruding solution originates, Anhydrite could precipitate as the solution penetrates the barrier.

8 Predictive calculations of chemical processes

8.1 Geochemical modelling of Salt concrete in contact to IP21 solution

The chemical evolution of IP21-solution penetrating Salt concrete can be depicted in a reaction path calculation. This means that a mass of IP21-solution equivalent to 1 kg of free water is reacted with an increasing mass of (formerly unreacted) Salt concrete. Thus, this procedure reproduces cascade leaching experiments.

As can be seen in the following figure, new mineral phases do form upon the intrusion of IP21-solution in Salt concrete, each one featuring a particular density. The resulting volume of neo-formed mineral phases (bottom), however, needs to be balanced against the volumes of those phases, which dissolve due to the reaction (top). Looking at the saturation indices it becomes obvious, that the CSH 0.8 phase, giving the Salt concrete its mechanical stability, is strongly under saturated - thus: unstable! – under the conditions imposed by the IP21-solution.

This calculation also gives the solid-solution-ratio at which CSH 0.8 attains equilibrium with the incoming solution and thus doesn't dissolve anymore. This threshold value can be tentatively given as 7 kg Salt concrete after reaction with IP21-solution equivalent to 1 kg of free water.

For a further analysis it will be necessary to identify reliable densities for the most relevant mineral phases present in this system. Unfortunately, for CSH 0.8 no density values are at hand at the time being.

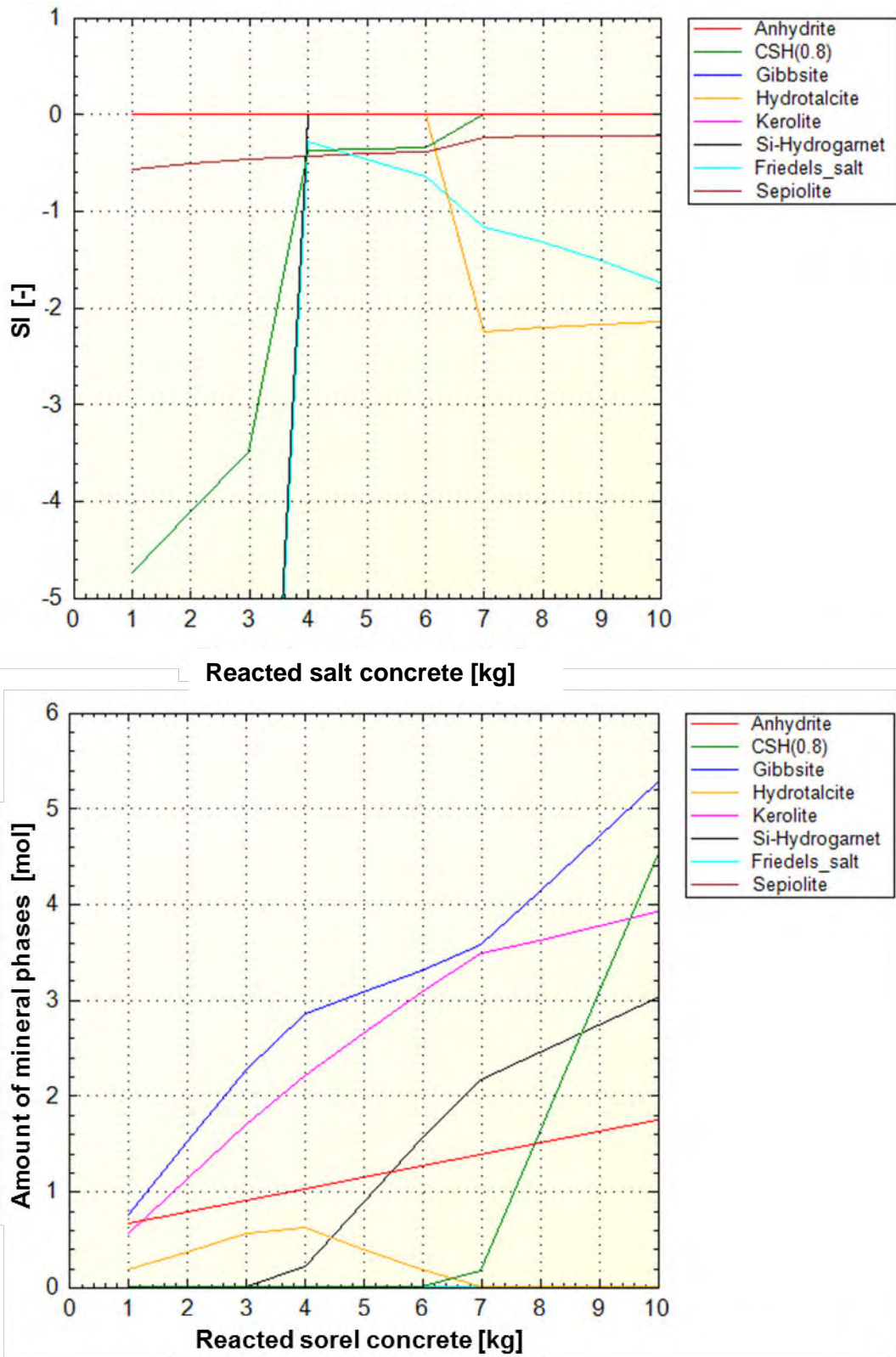


Fig. 8.1 Reaction of Salt concrete with IP21-solution. Top: saturation indices of selected mineral phases, Bottom: precipitated phases. "SI" describes the saturation index.

However, these predictions still need to be regarded with caution. They are based on the released THEREDA-database R-06, which is subject to further refinement. Furthermore, these calculations do not take kinetic effects into account, which are especially important for Ca-sulphate- and Si-containing phases.

8.2 Geochemical modelling of MgO based concretes in contact to brines

Recent findings indicated that in an initial phase of reaction between Sorel concrete and NaCl-solution Brucite is formed as a gel-like phase, which can be identified macroscopically, but due to its amorphous state cannot be detected by XRD. In a later state geochemical modelling predicted the formation of Mg-Oxichloride /MEY/HER 14/. This finding is supported by more recent model calculations.

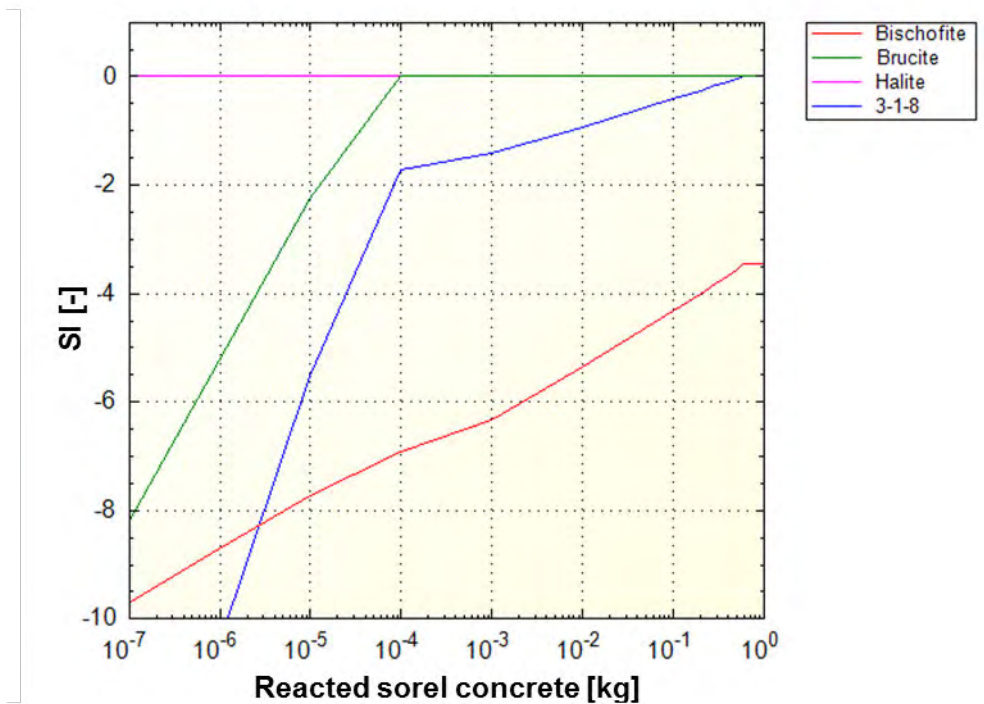


Fig. 8.2 Evolution of mineral saturation indices during the reaction of NaCl-solution with Sorel concrete

Fig. 8.3 shows modelled intrusion of a NaCl-brine to a Salt concrete structure. The figure represents a concrete sealing element which is penetrated by NaCl-solution on the left side. Hence, left part of diagram describes phase composition after reaction with solution and the right part describes the concrete before contact to NaCl-solution. It is

evident from the above figure, that upon intrusion of NaCl-solution into Sorel concrete, the phase 3-1-8 which is responsible for the mechanical strength of the material deteriorates. According to this calculation, 3-1-8 will begin to dissolve as soon as a mass of free water has reacted with the concrete (dissolving Na, Mg, and Na) which is twice as high as the reacted mass of concrete.

This picture doesn't change significantly if it is considered that real NaCl-solutions may contain certain amounts of CaSO_4 due to equilibration with Anhydrite.

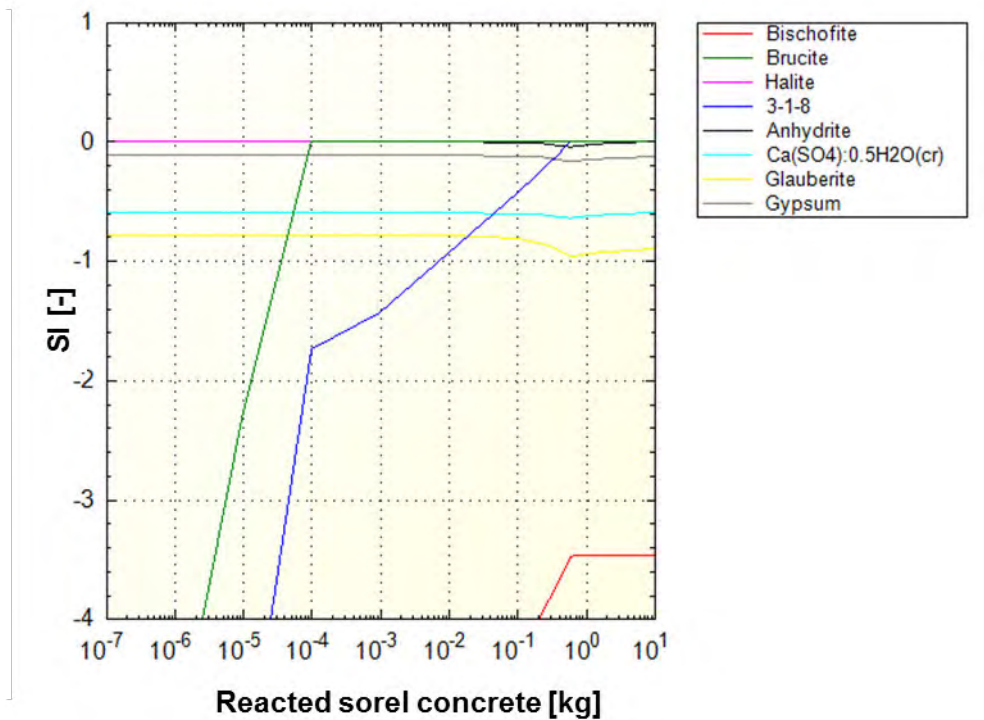


Fig. 8.3 Evolution of mineral saturation indices during the reaction of NaCl- CaSO_4 -solution with Sorel concrete

The only difference is that at high solid-solution-ratios the solution is saturated with respect to Anhydrite in addition to Brucite, 3-1-8, and Halite.

As with Salt concrete, these results must be further refined by consideration of the volume balance.

8.2.1 Preliminary modelling results of cascade experiments in comparison to laboratory results

This chapter describes the present state of reaction path modelling compared with experimental results of cascade experiments in the system Sorel concrete/NaCl-solution. Modelling shows only preliminary results. A better understanding of real reaction processes and kinetic effects is essential for an improved adaption of modelling.

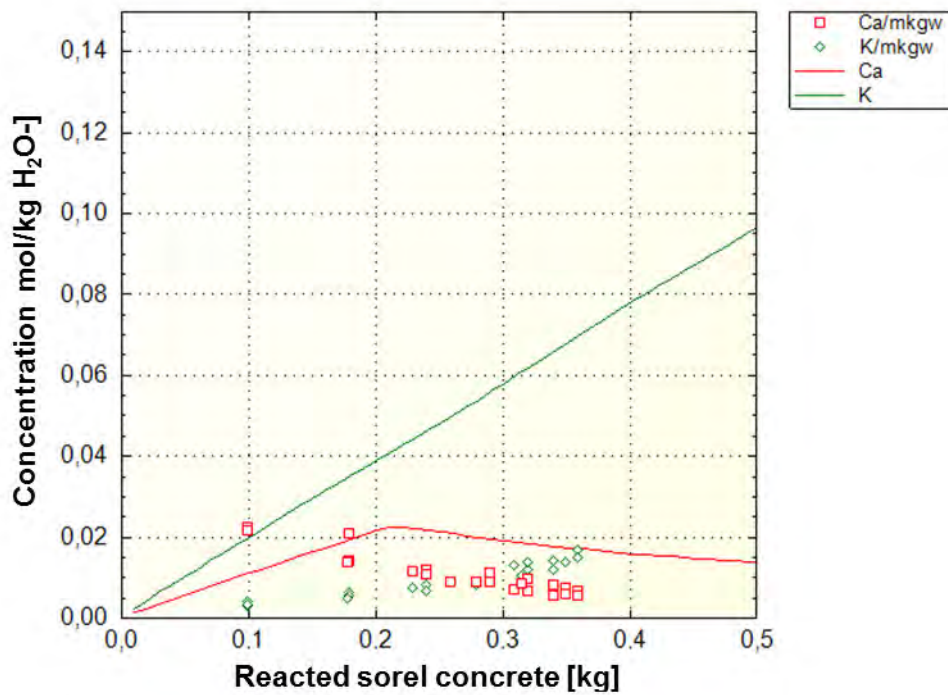


Fig. 8.4 Comparison of experimental results (points) and modelling (curves) for elements calcium and potassium in solution during cascade experiments

Fig. 8.4 describes the development of calcium and potassium concentrations in the reacted solution for each cascade. Clear differences between modelling and experimental results exist currently. Calcium concentrations are highest in cascade one and afterwards concentrations decrease continuously in experiments. Highest calcium concentration in modelling is first reached after cascade two and decreases afterwards. The values of both maxima are nearly identical. Probably kinetic effects need to be considered by modelling. The amount of potassium concentrations is clearly higher in modelling than in experiments. It can be assumed that less potassium is dissolved in

experiments than in the unreacted Sorel concrete is included, probably caused by an unknown K-phase.

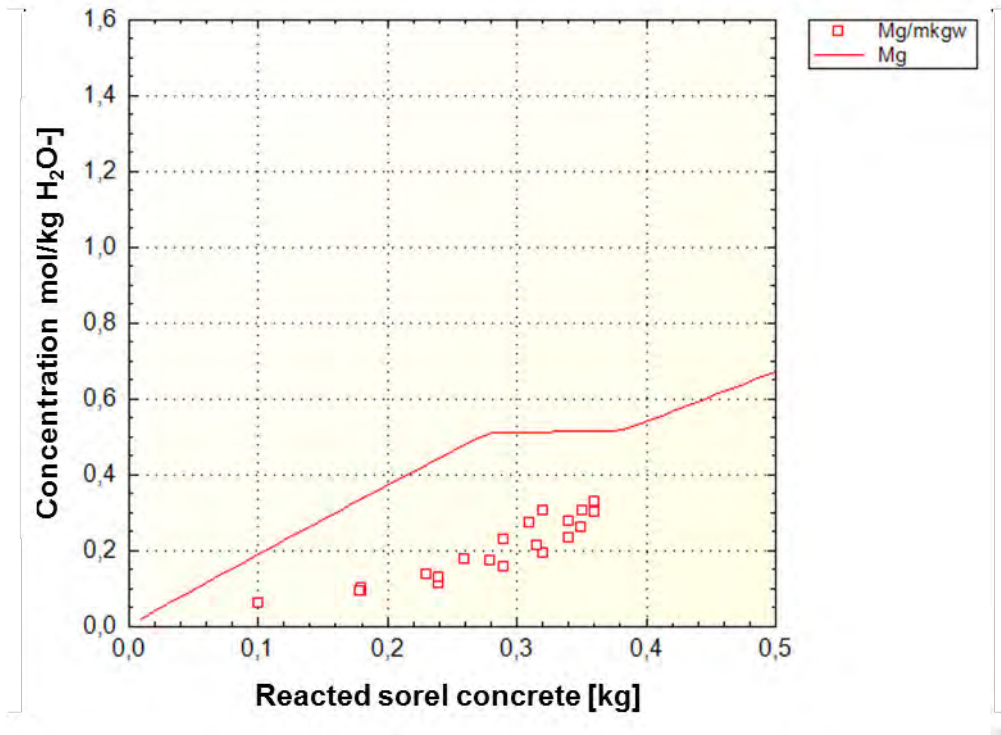


Fig. 8.5 Comparison of experimental results (points) and modelling (curves) for element magnesium in solution during cascade experiments

Comparison of development of magnesium concentrations shows that concentration increases faster in modelling than in laboratory. But it is noticeable that concentrations in experiments increase time-delayed nearly in parallel to calculated concentrations. Maybe this circumstance is caused by kinetic inhibition of dissolution of magnesium or by an overrating of magnesium solubility in the database.

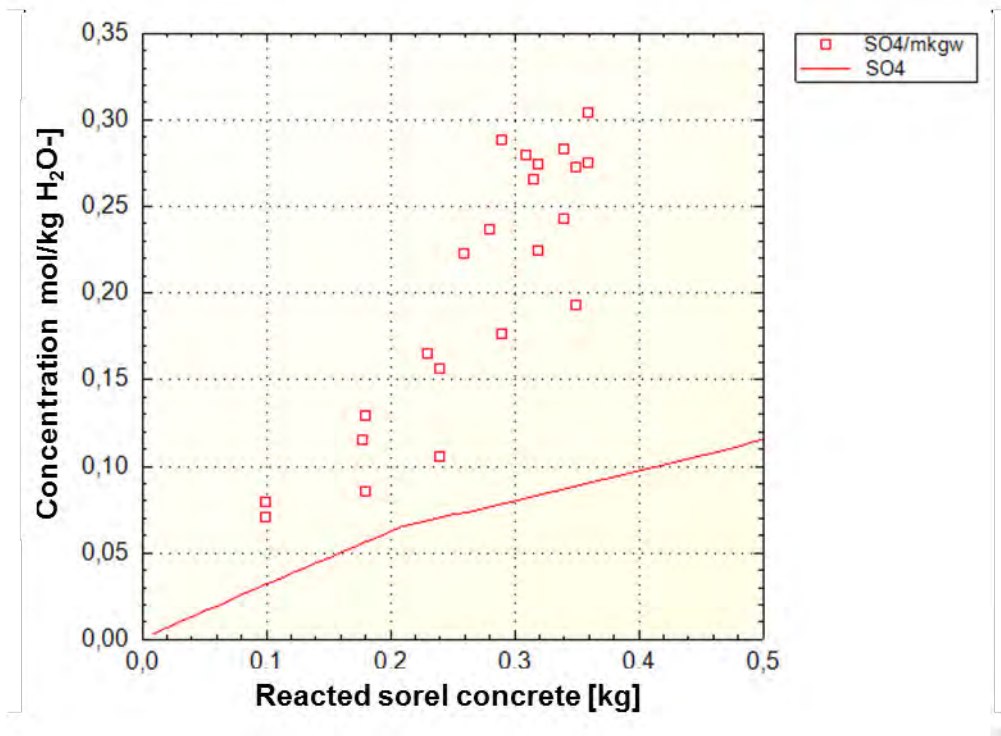


Fig. 8.6 Comparison of experimental results (points) and modelling (curves) for sulphate in solution during cascade experiments

Fig. 8.6 shows the development of sulphate concentrations in the solution. Concentrations of laboratory experiments are significant higher than calculated sulphate concentrations. It is assumed that used Sorel concrete in laboratory includes a further phase, which involves sulphate and is currently not considered by definition of the Sorel concrete phase in modelling.

9 Conclusions

This report presents the work related to the LAVA project that was also performed by GRS under WP 3 task 2 and WP 5 task 1 as part of the European project DOPAS and related to the LAVA-2 project. Works aim to investigate the sealing capacity of Salt and Sorel concrete with respect to geo-chemical long-term safety under conditions in rock salt.

Aqueous solutions approaching a repository in rock salt exhibit high ionic strengths and are saturated with respect to salt minerals constituting the host rock. These solutions have the potential to corrode cement-based sealing materials such as Salt and Sorel concrete. To give a predication for the long-term stability of cement based sealing elements geochemical processes need to be well known. Therefore a comprehensive geo-chemical laboratory program is currently being carried out.

Investigations were focused to corrosion of Salt and Sorel concrete in contact to NaCl- and Mg-rich-solutions. Each concrete has been investigated with contact to both solutions in various types of experiments.

Batch-experiments (section 5.1 and 6.1) were carried out for the investigation of the equilibration of concrete with solution. Time for the attainment of approximate equilibrium between powdered concrete and solution, the evolution of solution and phase composition of concrete was determined in these experiments. Sorel concrete in contact with NaCl-solutions features dissolution of stabilizing 3-1-8-phases. Contrary to expectations a change in solution composition could be observed in contact with Mg-rich-solution. Salt concrete tends to an opposite behaviour and is stable in NaCl-solution and corrodes in Mg-rich-solution. Batch-experiments confirmed this.

Cascade experiments (section 6.2.1) with Sorel concrete and NaCl-solution confirm the dissolution of 3-1-8-phase of Sorel concrete.

Pilot tests of diffusion experiments (section 6.3.1) were successfully done for Sorel concrete. Tests were performed with 1, 2 and 3 cm samples in height and provide diffusion coefficients for Sorel concrete. However the tests showed that there is a dependence of the velocity of diffusion to the height of the sample. Probably this phenomenon results from the diffusion at the grain boundary without diffusion in the concrete matrix in very small and inhomogeneous samples. Hence it is necessary to exe-

cute the main tests with 3 cm samples in order to exclude diffusion only at the grain boundaries. Pilot diffusion tests with Salt concrete are still in progress because a saturation of Salt concrete could not be accomplished yet.

In advection experiments (section 5.4 and 6.4) corrosion to solid Sorel concrete samples was investigated. Sorel concrete samples were exposed to an injection pressure of NaCl- respectively Mg-rich-solution at one end face. Flowed through solution was selected at the outflowing end face and permeability was calculated by Darcy's law. This is in accordance with findings in the batch experiments: in all Sorel concrete samples which were exposed to NaCl-solution permeability could be detected after seven to sixty days and permeability increased clearly. Experiments with Mg-rich-solutions have showed no flux over 200 days. Only one sample had a measureable permeability after circa 50 days but permeability remained constant at a small level for next 300 days. Maybe this sample had a well-connected pore system before start of advection experiment. After one year for all samples a breakthrough of solution was observed with Mg-rich-solution. Permeability was around $1 \cdot 10^{-19} \text{ m}^2$ to $3 \cdot 10^{-19} \text{ m}^2$ for all samples. Only the sample which percolated very early showed an increase of permeability meanwhile. But permeability decreased to its initial level in further progress. It needs to be clarified if this increase derives from process of corrosion or other effects.

Furthermore advection experiments with combined samples were executed (section 6.4). Permeability measurements of a combined sample of Sorel concrete surrounded with rock salt showed that a flowing through with Mg-rich-solution generates an increase of permeability resulting from a flow path along the contact zone. It is currently not clarified if the flowing path results from corrosion of Sorel concrete or from dissolution of rock salt.

A comparison of modelling and experimental results of cascade experiments shows differences between element concentrations in solution by modelling and laboratory experiments. For an improved agreement between modelling and experiments corrosion processes need to be investigated by further experiments and analysis and kinetic effects need to be understood better.

In general investigations have confirmed earlier assumptions about the corrosion behaviour of Salt concrete in contact to NaCl- and Mg-rich solutions and to Sorel concrete in contact to NaCl-solutions. But laboratory tests also raised some questions which

need to be investigated in further tests. In context with Sorel concrete secondary phases which develop after reaction with NaCl-solution need to be identified. Additional processes in contact with Mg-rich-solution need to be understood. In Salt concrete the process of closure of the contact zone between concrete and rock salt should be further investigated.

10 Zusammenfassung

In diesem Bericht werden zusammenfassend die Ergebnisse aus dem LAVA und LAVA-2-Projekt dargestellt. Das LAVA-Projekt wurde von der GRS im Rahmen des EU-Projektes DOPAS durchgeführt. Die Arbeiten beziehen sich auf die Vertikalprojekte 3, Arbeitspaket 2 und Vertikalprojekt 5, Arbeitspaket 1. Ziel der Forschungsarbeiten ist die Untersuchung des Abdichtungsvermögens von Salz- und Sorelbeton in Hinblick auf die geochemische Langzeitstabilität unter salinaren Bedingungen.

Wässrige Lösungen, die einem Salzstock zutreten, sättigen sich mit Salzmineralen auf, sodass hochsalinare Lösungen entstehen können. Die Zusammensetzung der Lösung hängt von der Mineralgemeinschaft des anstehenden Salzstockes ab. Abhängig von der Lösungszusammensetzung können diese hochsalinaren Lösungen eine Korrosion des Salz- bzw. Sorelbeton hervorrufen. Um eine Vorhersage über die Langzeitstabilität eines Dammbauelements geben zu können, müssen die geochemischen Prozesse verstanden werden. Aus diesem Grund wurde ein umfangreiches geochemisches Laborprogramm zur Untersuchung von Salz- und Sorelbeton durchgeführt.

Die Untersuchungen konzentrierten sich auf Salz- und Sorelbeton in Kontakt zu NaCl- und Mg-reichen-Lösungen.

Die Batchexperimente (Kapitel 5.4 und 6.4) wurden durchgeführt um zunächst das Gleichgewicht der beiden Betone in Kontakt zu den unterschiedlichen salinaren Lösungen zu untersuchen. Ziel dieser Versuche war es im Wesentlichen, die Equilibrierungszeit zwischen dem gemahlten Beton und der Lösung zu ermitteln. Dazu wurde die Entwicklung der Lösungs- und Feststoffzusammensetzung über einen bestimmten Zeitraum analysiert. Aus den Ergebnissen konnte abgeleitet werden, wann die signifikanten Umlöseprozesse im jeweiligen System abgeschlossen sind. Die Ergebnisse bestätigten für den Sorelbeton in Kontakt mit NaCl-Lösung die Auflösung der charakteristischen und stabilisierenden 3-1-8-Phase. Im Systeme Sorelbeton / Mg-reiche Lösung konnte entgegen den Erwartungen ebenfalls eine Änderung der Lösungszusammensetzung identifiziert werden. Salzbeton hingegen zeigte sich stabil in NaCl-Lösungen und korrodiert in Mg-reichen Lösungen.

Die Kaskadenexperimente (Kapitel 6.2.1) mit Sorelbeton und NaCl-Lösung bestätigen die Auflösung der 3-1-8-Phase analog zu den Batchexperimenten.

Des Weiteren wurden Vorversuche für Through-Diffusion-Experimente durchgeführt (Kapitel 6.3.1). In diesen Experimenten sollte ermittelt werden, welche Prüfkörperhöhe (1 cm, 2 cm oder 3 cm) sich am besten für die Ermittlung von Diffusionskoeffizienten eignet. Die Ergebnisse am Sorelbeton zeigen, dass eine Abhängigkeit zwischen der Höhe der Prüfkörper und dem Diffusionskoeffizienten besteht. Vermutlich ist dieses Phänomen auf die Inhomogenität des Sorelbetons zurückzuführen, weil die Diffusion entlang von Korngrenzen schneller erfolgt als in der Zementmatrix. Folglich kann die Korrosion in den 1 cm Proben zu einem höheren Anteil auf Korngrenzen erfolgen und ist somit auch schneller als in den 2 und 3 cm Proben. Aus diesem Grund sollen die folgenden Through-Diffusion-Experimente an Prüfkörpern mit 3 cm Höhe durchgeführt werden, um realistischere Diffusionskoeffizienten zu erhalten. Die Vorversuche an Salzbeton befinden sich derzeit immer noch in der ersten Versuchsphase, da eine Auf-sättigung der Prüfkörper bislang nicht erfolgt ist.

In Advektionsexperimenten (Kapitel 5.4 und 6.4) wurde die Korrosion von Sorelbeton in Kontakt zu NaCl- bzw. Mg-reichen-Lösungen unter advektivem Lösungsfluss untersucht. Dazu wurden Sorelbetonprüfkörper mit einem Lösungsdruck an einer Stirnfläche beaufschlagt und die durchgeflossene Lösung an der gegenüberliegenden Stirnfläche aufgefangen. Über das Gesetz von Darcy wurde anschließend die Permeabilitätsentwicklung ermittelt. Die Ergebnisse bestätigen die Erkenntnisse aus den Batchexperimenten: An den Prüfkörpern, die mit einer NaCl-Lösung durchströmt wurden, konnte nach sieben bis sechzig Tagen ein Lösungsdurchbruch und danach ein rascher Anstieg der Permeabilität auf ca. $1 \cdot 10^{-17} \text{ m}^2$ identifiziert werden. Bei den Prüfkörpern, die mit Mg-reicher-Lösung beaufschlagt wurden, konnte hingegen erst nach 200 Tagen in einem Teil der Prüfkörper ein Durchbruch der Lösung festgestellt werden und erst nach einem Jahr in allen Prüfkörpern. Lediglich ein Prüfkörper zeigte bereits nach 50 Tagen einen Durchfluss der Mg-reichen-Lösung. Die Permeabilität blieb aber über die nächsten 300 Tage konstant. Zwischenzeitlich konnte ein kurzer Anstieg der Permeabilität festgestellt werden. Danach fiel die Permeabilität jedoch wieder auf ihr Ausgangsniveau. Vermutlich ist die früh messbare Permeabilität in diesem Prüfkörper mit einem gut vernetzen Porensystem zu erklären. Die Permeabilität in den mit Mg-reicher-Lösung durchströmten Prüfkörpern lag bei $1 \cdot 10^{-19} \text{ m}^2$ bis $3 \cdot 10^{-19} \text{ m}^2$.

Weiterhin wurden Advektionsversuche an kombinierten Prüfkörpern (Kapitel 6.4) durchgeführt. Die Permeabilitätsuntersuchungen an einer Sorelbetonprobe, die in Steinsalz eingefasst war, haben gezeigt, dass die Durchströmung der Kontaktfläche

mit Mg-reicher-Lösung zu einem Anstieg der Permeabilität führt. Aktuell ist noch nicht geklärt, ob dies aus einer Korrosion des Sorelbeton oder des anstehenden Steinsalzes resultiert.

Ein Vergleich zwischen der Modellierung der Kaskadenversuche und den experimentell ermittelten Werten der Lösungsentwicklung zeigen aktuell Abweichungen zwischen den Elementkonzentrationen. Um eine bessere Übereinstimmung zwischen der Modellierung und den experimentellen Daten zu erhalten, ist eine ausführliche Analyse der der Feststoffphasen sowie eine Untersuchung kinetischer Effekte nötig.

Insgesamt haben die Untersuchungen die bisherigen Annahmen zur Korrosion von Salzbeton in Kontakt mit NaCl- und Mg-reichen Lösungen sowie für Sorelbeton mit NaCl-Lösung bestätigt. Allerdings sind durch die Laboruntersuchungen auch weitere Fragestellungen aufgetan worden, die in weiteren Versuchen untersucht werden sollten. Bei der Korrosion von Sorelbeton mit NaCl-Lösung sind möglicher Weise noch nicht alle sich bildenden Phasen eindeutig identifiziert worden und auch die Prozesse im System Sorelbeton mit Mg-reicher Lösung sind nicht vollständig verstanden. Ebenso ergeben sich Fragen aus dem Prozess des Schließens der Kontaktfuge zwischen Steinsalz und Salzbeton bei Durchströmung mit einer NaCl-Lösung.

References

- /BIC 68/ Biczók, I. (1968): Betonkorrosion – Betonschutz. Bauverlag, Wiesbaden.
- /BON 92/ Bonen, D. (1992): Composition and appearance of magnesium silicate hydrate and its relation to deterioration of cement-based materials. J. Am. Ceram. Soc. (75), p 2904-2906.
- /BRE 05/ Brew, D.R.M., Glasser, F.P. (2005): Synthesis and characterisation of magnesium silicate hydrate gels. Cement. Concr. Res. (35), S. 85-98.
- /DIN/FRE 10/ Dinnebier, R. E.; Freyer, D.; Bette, S.; Oestreich, M. (2010): $9\text{Mg}(\text{OH})_2 \cdot \text{MgCl}_2 \cdot 4\text{H}_2\text{O}$, a High Temperature Phase of the Magnesia Binder System. Inorganic Chemistry (49), 9770-9776.
- /ENG 08/ Engelhardt, H.J. (2008): Mikroskopische Untersuchungen des Kontaktbereiches von Steinsalz und Salzbeton – ASSE Vordamm, Deutschland 2008
- /FRE 15/ Freyer, D. (2015): Instiut für anorganische Chemie, TU Bergakademie Freiberg, personal communication (05.06.2015)
- /GRA 96/ Grattan-Bellew, P.E., Beaudoin, J.J., Valee, V.G. (1996): Delayed ettringite formation: effect of clinker particle size and composition on expansion of mortar bars. – In: Cohen, M., Mindess, S., Skalny, J.: Materials science of concrete: The Sydney Diamond Symposium. American Ceramic Society, Westerville, OH, S. 295-308.
- /HAS 03/ Hagemann, S. und Meyer Th, (2003): Unsicherheits- und Sensitivitätsanalyse zur Korrosion von Salzbeton durch saline Lösungen. GRS-A-3458, Project Morsleben, PSP Element 9M 232 200 11, 114 p.
- /HEA 99/ Hearn, N., Young, F. (1999): W/C ratio, porosity and sulphate attack – a review. In: Marchand, J., Skalny, J.: S. 189-205.
- /HER 96/ Herbert, H.-J. und Mönig, J. (1996): Exemplarische Untersuchungen von Wechselwirkungsreaktionen UTD-relevanter chemisch-toxischer Abfälle mit hochsalinaren Lösungen. GRS Report, GRS-126.

- /HER 98/ Herbert, H.-J. und Meyer, Th. (1998): Untersuchung und Modellierung des Lösungsverhaltens von tragendem Versatz im ERAM. GRS Report, AG-Nr. 1512, 71.
- /HER 12/ Herbert, H.-J. (2012): Entwicklung chemisch-hydraulischer Modelle für die Prognose des Langzeitverhaltens von Sorelbeton in Salzformationen, Anlage A Vorhabensbeschreibung
- /HEW 98/ Hewlett, P.C. (1998): Lea's Chemistry of Cement and Concrete. Fourth Ed. Arnold, London.
- /KAN 61/ Kancepolskij, I.S., Žabiskij, M.S., Sevjakov, P.E. (1961): In: "Korrozija cementov i mery bor'by s nej", Taschkent. Zitiert in /KIN 68/.
- /KIN 68/ Kind, W.W. (1968): Zement- und Betonkorrosion durch Magnesiumsalzlösungen. In: Silikatchemische Probleme und Korrosion des Betons. 2. Internationale Baustoff- und Silikattagung Weimar. Schriften der Hochschule für Architektur und Bauwesen Weimar (6), S. 124-140.
- /MAT 12/ Mattigod, S.V.; Wellman, D.M.; Bovaird, C.C.; Parker, K.E.; Recknagle, K.P.; Clayton, L.; Wood, M.I. (2012): Diffusion of Radionuclides in Concrete and Soil
- /MEH 00/ Mehta, K. (2000): Sulphate Attack on Concrete: Separating Myths from Reality. Concrete International (8), S. 57-61.
- /MEH 91/ Mehta, P.K. (1991): Concrete in the marine environment. Elsevier.
- /MEY 99/ Meyer, Th. und Herbert, H.-J. (1999): Geochemische Modellierung der Betonkorrosion - International Symposium Environment 2000. Halle, Sept. 22.-25th. 1999.
- /MEY 02/ Meyer Th., Herbert, H.-J, Schmidt-Döhl, F., Dettmer F. (2002): Endlager Morsleben – Zementkorrosion. GRS Report, GRS-A-3034, PSP-Element 9M 212 200 11/12, 221 S.
- /MEY 03a/ Meyer Th., Herbert, H.-J, Schmidt-Döhl, F. (2003): Endlager Morsleben – Korrosion von Salzbeton durch salinaren Lösungen. GRS Report, GRS-A-3170. PSP-Element 9M 212 200 11/12, 210 S.

- /MEY 03b/ Meyer Th., Herbert, H.-J, Schmidt-Döhl, F. (2003): Endlager Morsleben – Korrosion zementhaltiger Materialien bei Mehrfachdurchströmung mit salinaren Lösungen. GRS Report, GRS-A-3150. PSP-Element 9M 212 200 11/12, 205 S.
- /MEY 03c/ Meyer Th. and Herbert H.-J. (2003): The long-term performance of cementitious materials in underground repositories for nuclear waste. International Congress on the Chemistry of Cements, Durban, South Africa, 2003, 10p.
- /MEY 04/ Meyer Th. (2004): Corrosion of cementitious materials under geological disposal conditions. CSNI/RILEM Workshop, Madrid, 15-16 March 2004, 10p.
- /MEY/HER 14/ Meyer, Th.; Herbert, H.-J. (2014): Full scale demonstration of plugs and seals (DOPAS). Deliverable D3.29 and D5.5. Status report on ELSA related laboratory tests and on process modeling activities. GRS - A – 3740.
- /MÜL 10/ Müller-Hoeppe, N. (2010): Untersuchungen der Kontaktzone am ASSE-Vordamm – Gesamtinterpretation, Deutschland 2010
- /NIE 14/ Niemeyer, M.; Wilhelm, S.; Hagemann, S.; Herbert, H.-J. (2014): Stilllegung ERAM - Zusammenfassende Auswertung von Experimenten und Modellrechnungen zur Korrosion von Salzbeton mit IP21-Lösung. BfS
- /PAR/APP 99/ Parkhurst, D. L.; Appelo, C. A. J. (1999): User's guide to PHREEQC (Version 2): A computer program for speciation, batch-reaction, one-dimensional transport, and inverse geochemical calculations.
- /POW 58/ Powers, T.C. (1958): Structure and physical properties of hardened Portland cement paste. J. Am. Ceram. Soc. (41), S. 1-6.
- /RUN/DIN 14/ Runčevski, T.; Dinnebier, R. E.; Freyer, D. (2014): Dehydration of the Sorel Cement Phase $3\text{Mg}(\text{OH})_2 \cdot \text{MgCl}_2 \cdot 8\text{H}_2\text{O}$ studied by in situ Synchrotron X-ray Powder Diffraction and Thermal Analyses. Z. anorg. allg. Chem. (640), 1521-3749.

- /SGL/GEN 11/ Sglavo, V. M.; Genua, F.; Conci, A.; Ceccato, R.; Cavallini, R. (2001): Influence of curing temperature on the evolution of magnesium oxychloride cement. *Journal of Materials Science* (46), 6726-6733.
- /SKA 02/ Skalny, J., Marchand, J., Odler, I. (2002): Sulphate attack on concrete. Spon Press, London.
- /TEI 09/ Teichmann, L., Meyer, T. (2009): Beschreibung der zur Verfüllung der Firstspalte ausgewählten Sorelbetone A1 und A1-560. Anlage 1, Germany
- /TEM 98/ Temuujin, J., Okada, K., MacKenzie, K.J.D. (1998): Role of water in the mechanochemical reactions of MgO-SiO₂ systems. *J. Solid State Chem.* (138), S. 169-177.
- /YAN 60/ Yang, J.C.-S. (1960): The system magnesia-silica-water below 300°C: I. Low-temperature phases from 100°C to 300°C and their properties. *J. Am. Ceram. Soc.* (43), S. 542-549.

Tables

Tab. 4.1	Composition of Salt concrete /MÜL 10/ (Source gives total mass of components to 100 % but by addition it is only 99.9 %. Probably this deviation is not significant in context to the uncertainty of measurements.).....	10
Tab. 4.2	Mechanical parameters of used Salt concrete /MÜL 10/	11
Tab. 4.3	Thermal properties of used Salt concrete /MÜL 12b/	14
Tab. 4.4	Composition of Sorel concrete A1 /TEI 09/	14
Tab. 4.5	Mechanical properties of Sorel concrete A1 /TEI 09/	15
Tab. 4.6	Thermal properties of Sorel concrete A1 (for samples dried at 60°C) /TEI 09/.....	16

Figures

Fig. 3.1	CSH-phases in Salt concrete covered by Halite; Friedel's salt (hexagonal plates) /MEY 03a/.....	7
Fig. 4.1	Salt concrete sample	11
Fig. 4.2	Sorel concrete sample	15
Fig. 5.1	Principle of cascade leaching experiments /HER 96/, /MEY 02/.....	18
Fig. 5.2	Experimental set-up of the batch/cascade experiment.....	19
Fig. 5.3	Layout of in-diffusion experiments	20
Fig. 5.4	Simplified construction of a diffusion cell.....	21
Fig. 5.5	Construction of an advection cell	22
Fig. 5.6	Experimental set up of advection experiment in laboratory	23
Fig. 5.7	Production of combined samples	24
Fig. 6.1	Phase composition of Sorel concrete A1 before contact with solution.....	27
Fig. 6.2	Phase composition of Sorel concrete A1 after 9, 11 and 18 days of contact with NaCl-solution	28
Fig. 6.3	Development of Cl, Na, Ca, K, Mg and sulphate concentrations in batch-experiments in the system Sorel concrete/NaCl-solution. Black bars describe errors of 5 %.....	29
Fig. 6.4	Phase composition of Sorel concrete after contact to Mg-rich-solution	30
Fig. 6.5	Development of Ca, K, Na, Sulphate, Cl and Mg concentrations in batch-experiments in the system Sorel concrete/Mg-rich-solution. Black bars describe errors of 5 %	31

Fig. 6.6	Phase composition of Salt concrete before contact with solution	32
Fig. 6.7	Phase composition of Salt concrete after contact to NaCl-solution	33
Fig. 6.8	Development of Cl, Na, Ca, K, Mg, sulphate, Al and Si concentrations in batch-experiments in the system Salt concrete/NaCl-solution. Black bars describe errors of 5 %.....	34
Fig. 6.9	Phase composition of Salt concrete after contact with a Mg-rich solution	35
Fig. 6.10	Development of Mg, Na, Cl, Ca, K and sulphate concentrations in batch-experiments in the system Salt concrete/Mg-rich-solution. Black bars describe errors of 5 %	36
Fig. 6.11	Development of Al and Si concentrations in batch-experiments in the system Salt concrete/Mg-rich-solution. Black bars describe errors of 5 %	37
Fig. 6.12	Development of density in cascade experiment with Sorel concrete and NaCl-solution	40
Fig. 6.13	Development of solution composition in cascade experiments with Sorel concrete and NaCl-solution. Black bars describe errors of 5 %.....	41
Fig. 6.14	Development of density in cascade experiment with Salt concrete and Mg-rich-solution	42
Fig. 6.15	Calculated penetration profiles by diffusive transport in concrete. Matrix permeability: 10^{-20} to 10^{-21} m ² . Diffusion coefficients of 10^{-13} , 10^{-14} and 10^{-15} m ² /s /HER 12/.....	43
Fig. 6.16	Samples in first phase of through-diffusion experiments before solutions were admitted. Sorel concrete (left) and Salt concrete (right)....	44
Fig. 6.17	Diffusion cell with inserted sample (left) and layout of through-diffusion experiments during phase 2 of experiment (right)	45

Fig. 6.18	Upper diagram: Cumulated mass of tracer lithium in diffusion experiments with Sorel concrete and NaCl-solution (blue) and Sorel concrete and Mg-rich-solution (green). Diagram below: Cumulated mass of tracer lithium (smaller scaling of y-axis). Black bars describe errors of 5 %.	46
Fig. 6.19	Upper Diagram: Cumulated mass of tracer caesium in diffusion experiments with Sorel concrete and NaCl-solution (blue) and Sorel concrete and Mg-rich-solution (green). Diagram below: Cumulated mass of tracer caesium (smaller scaling of y-axis). Black bars describe errors of 5 %.	47
Fig. 6.20	Development of permeability of Sorel concrete samples in contact to NaCl-solution (vertical lines mark time steps in which flow through of solution has been stopped, further reaction between concrete and solution has been awaited and afterwards change of permeability and solution composition was investigated)	49
Fig. 6.21	Development of solution composition in advection experiments with NaCl-solution. Circlet points mark measurements after stop of flow through of solution. Black bars describe errors of 5 %.	50
Fig. 6.22	Development of permeability of Sorel concrete samples in contact to Mg-rich-solution. The reason for higher values of permeability of sample AS-36-2 (marked by the interrogation mark) is not clarified yet....	52
Fig. 6.23	Development of solution composition in advection experiments with Mg-rich-solution	53
Fig. 6.24	Coated sample in an isostatic cell (left) and cell arrangement (right)	55
Fig. 6.25	Work curve: Development of permeability of a combined sample (Sorel concrete/rock salt). Permeability increases directly after start of flowing through with Mg-rich-solution.	55
Fig. 6.26	Combined sample (Sorel concrete/rock salt) after flowing through with Mg-rich-solution. At the contact zone is clearly a crack to identify	56

Fig. 6.27	Work curve: Development of permeability of a combined sample (Salt concrete/rock salt). Phase 1: Compaction of sample without solution – no significant decrease of permeability to gas. Phase 2: Flowing through of NaCl-solution with a very small surrounding pressure – clearly decrease of permeability to solution.....	57
Fig. 6.28	Development of permeability of a combined sample (Salt concrete/rock salt). Phase 1: Flow of NaCl-solution and compaction of sample. Phase 2: Change to Mg-rich-solution and decrease of permeability. Phase 3: Increase of permeability	58
Fig. 7.1	Schematic representation of the chemical corrosion processes in Salt concrete due to the interaction with Mg-, SO ₄ - and Cl-rich salt solutions (left) diffusive matrix corrosion, (right) advective matrix corrosion on cracks (in /HAS 03/ modified after /BON 92/)	60
Fig. 7.2	Permeability changes of M2-4 Salt concrete in contact with IP21 solution at rising numbers of pore volume exchange /MEY 03b/	61
Fig. 8.1	Reaction of Salt concrete with IP21-solution. Top: saturation indices of selected mineral phases, Bottom: precipitated phases. “SI” describes the saturation index.	65
Fig. 8.2	Evolution of mineral saturation indices during the reaction of NaCl-solution with Sorel concrete	66
Fig. 8.3	Evolution of mineral saturation indices during the reaction of NaCl-CaSO ₄ -solution with Sorel concrete	67
Fig. 8.4	Comparison of experimental results (points) and modelling (curves) for elements calcium and potassium in solution during cascade experiments.....	68
Fig. 8.5	Comparison of experimental results (points) and modelling (curves) for element magnesium in solution during cascade experiments	69

Fig. 8.6 Comparison of experimental results (points) and modelling (curves)
for sulphate in solution during cascade experiments..... 70

GRS-A-3869

Druckexemplare:

Projektträger Karlsruhe (PTKA)

Michael Bühler 5 x

GRS

Bibliothek Köln	1 x
Bibliothek Braunschweig	1 x
Bereichsleiter (moe, prg)	2 x
Abteilungsleiter (cza, fap)	2 x
Projektleiter (moo)	1 x
Autoren (huw, jky, met)	3 x

Gesamt 15 x

PDF-Version:

PTKA (Bühler)

GRS

Geschäftsführer	(suw, stj)
Bereichsleiter	(fil, kre, moe, prg, san, stc, stu)
Projektleiter	(moo)
Projektcontrolling	(bit)
Autor(en)	(huw, jky, met)
TECDO	(wev)

**Gesellschaft für Anlagen-
und Reaktorsicherheit
(GRS) gGmbH**

Schwertnergasse 1

50667 Köln

Telefon +49 221 2068-0

Telefax +49 221 2068-888

Forschungszentrum

85748 Garching b. München

Telefon +49 89 32004-0

Telefax +49 89 32004-300

Kurfürstendamm 200

10719 Berlin

Telefon +49 30 88589-0

Telefax +49 30 88589-111

Theodor-Heuss-Straße 4

38122 Braunschweig

Telefon +49 531 8012-0

Telefax +49 531 8012-200

www.grs.de